Cachd1 interacts with Wnt receptors and regulates neuronal asymmetry in the zebrafish brain

Authors: Gareth T. Powell[1,2]†, Ana Faro[1]†, Yuguang Zhao[3]*†, Heather Stickney[1,4,5]†, Laura Novellasdemunt[6,7], Pedro Henriques[1], Gaia Gestri[1], Esther Redhouse White[1], Jingshan Ren[3], Weixian Lu[3], Rodrigo M. Young[1,8,9], Thomas A. Hawkins[1], Florencia Cavodeassi[1,10], Quenten Schwarz[8], Elena Dreosti[1], David W. Raible[4], Vivian S. W. Li[6], Gavin J. Wright[2,11], E. Yvonne Jones[3]*, Stephen W. Wilson[1]*

Affiliations:

[1]Cell and Developmental Biology, University College London; London, WC1E 6BT, UK.

[2]Wellcome Trust Sanger Institute; Cambridge CB10 1SA, UK.

[3]Division of Structural Biology, Wellcome Centre for Human Genetics, University of Oxford; Oxford, OX3 7BN, UK.

[4]Departments of Otolaryngology-HNS and Biological Structure, University of Washington; Seattle, WA 98195-7420, USA.

[5]Ambry Genetics; Aliso Viejo, CA 92656, USA.

[6]The Francis Crick Institute; London, NW1 1AT, UK.

[7]Institute for Research in Biomedicine (IRB Barcelona), The Barcelona Institute of Science and Technology; 08028, Barcelona, Spain

[8]Institute of Ophthalmology, University College London; London, EC1V 9EL, UK.

[9]Center for Integrative Biology, Facultad de Ciencias, Universidad Mayor; Camino La Piramide 5750, 8580745, Santiago, Chile.

[10]St. George's, University of London; London, SW17 0RE, UK.

[11]Department of Biology, Hull York Medical School, York Biomedical Research Institute, University of York; York, YO10 5DD, UK.

*Corresponding author. Email: s.wilson@ucl.ac.uk (S. W. W.), yvonne.jones@strubi.ox.ac.uk (E. Y. J.), yuguang.zhao@strubi.ox.ac.uk (Y. Z.)

†These authors contributed equally to this work

Abstract:

Neurons on left and right sides of the nervous system often show asymmetric properties, but how such differences arise is poorly understood. Genetic screening in zebrafish revealed that loss-of-function of the transmembrane protein Cachd1 resulted in right-sided habenula neurons adopting left-sided identity. Cachd1 is expressed in neuronal progenitors, functions downstream of asymmetric environmental signals, and influences timing of the normally asymmetric patterns of neurogenesis. Biochemical and structural analyses demonstrated that Cachd1 can bind simultaneously to Lrp6 and Frizzled family Wnt co-receptors. Consistent with this, *lrp6* mutant zebrafish lose asymmetry in the habenulae, and epistasis experiments support a role for Cachd1 in modulating Wnt pathway activity in the brain. These studies identify Cachd1 as a conserved Wnt receptor-interacting protein that regulates lateralized neuronal identity in the zebrafish brain.

Main Text:

The nervous systems of bilaterian animals are left-right (LR) asymmetric with respect to neuroanatomy, processing of information, and control of behavior (*1-5*). Within vertebrates, the epithalamus shows evolutionarily conserved LR asymmetries (*6, 7*). In zebrafish, the epithalamic dorsal habenulae (dHb) comprise a medial (dHb_M) domain that is larger on the right and a lateral (dHb_L) domain that is larger on the left (*8-10*). Afferent innervation is also asymmetric, with mitral cells innervating the right dHb and parapineal neurons innervating the left dHb (*5, 11, 12*). Functional asymmetry mirrors neuroanatomy in young fish with, for example, light activating predominantly left-sided dHb_L neurons and odor activating a higher proportion of right-sided dHb_M neurons (*13, 14*).

Development of epithalamic asymmetry is dependent on sequential interactions between cell groups that coordinate lateralization of circuit components (*15-17*). Genetic analyses in zebrafish have revealed roles for Wnt signaling in this process. For example, fish with compromised function of the scaffolding protein Axin1 have symmetric habenulae with right-sided character (*18*) whereas habenulae are symmetric with left-sided character in fish lacking function of the Tcf7l2 transcriptional effector (*19*). Wnt signaling also affects the balance between proliferation and neurogenesis (*20, 21*) suggesting complex regulation of pathway activity during epithalamic development. More generally, Wnt signaling is involved in a wide array of biological processes during embryonic development, throughout life, and in many disease states (*22-25*). Through studying the role of Wnt signaling in the establishment of brain asymmetry, we identified Cachd1 as a transmembrane component of this highly conserved and multifunctional signaling pathway.

rorschach^{u761} mutants show symmetric habenulae owing to a lesion in *cachd1*

To identify genes potentially involved in establishing brain asymmetry, we screened zebrafish embryos for *N*-ethyl-*N*-nitrosourea (ENU)-induced mutations (*19*) that alter asymmetric habenular expression of *kctd12.1* (*8*) and identified the homozygous viable *rorschach*^{u761} mutant (*rch*). In 4 dpf (days post fertilization) mutant larvae, *kctd12.1* expression in the right habenula was increased, reaching a similar degree as on the left, suggesting that both habenulae exhibit left-sided character (Fig. 1A). Other than this fully penetrant habenular phenotype, *rch* mutants were morphologically indistinguishable from wildtypes with normal asymmetry of the viscera.

Mapping placed the *rch* mutation in a 0.28 Mb interval on chromosome 6, and sequencing identified a nonsynonymous single-base pair change in *cachd1* that switched a nonpolar valine to an acidic aspartic acid (V1122D). *cachd1* encodes a 1290 amino acid type I transmembrane protein with dCache and von-Willebrand factor type A (VWA) domains; the V1122D missense mutation occurs within the transmembrane domain (Fig. 1B) and disrupts membrane localization of the protein (Fig. 1C and fig.S1). Embryos homozygous for a likely null mutation in *cachd1* (*sa17010*), producing no detectable Cachd1 protein (fig. S1 and table S1), showed the same habenular double left-phenotype, as did transheterozygote *cachd1*^{u761}/*cachd1*^{sa17010} mutants (Fig. 1D and fig. S2) and embryos injected with splice-blocking *cachd1* morpholinos (fig. S3). Habenular asymmetry was partially restored in homozygous *cachd1*^{u761} mutants expressing exogenous Cachd1 from a heat shock promoter during the period of habenular neurogenesis [*Tg(HSE:cachd1, EGFP)w160*] (fig. S4). By contrast, expressing Cachd1-enhanced green fluorescent protein (EGFP) in postmitotic neurons did not rescue the *rorschach* phenotype [*Tg(neurod1:cachd1-EGFP)w162*] (fig. S4). These results show that loss of Cachd1 function during habenular neurogenesis is responsible for the symmetric habenular phenotype.

Cachd1 is expressed in neuroepithelial cells along the dorsal midline of the brain

To determine the spatiotemporal pattern of *cachd1* expression, we performed colorimetric (fig. S5) and double fluorescent in situ hybridization using epithalamic and habenula markers (Fig. 1E and fig. S6) and immunohistochemistry using an antibody raised against the extracellular domain of zebrafish Cachd1 (Fig. 1F and fig. S1). Before neuronal differentiation, *cachd1* is expressed broadly within the dorsal diencephalon colocalizing with *dbx1b*, a marker of habenula neuron precursors (fig. S6) (*26*). During the period of habenular neurogenesis (*27, 28*), *cachd1*/Cachd1 expression becomes restricted to a proliferative neuroepithelial domain adjacent to mature habenula neurons (fig. S7). Although *cachd1* mutants only show an overt mutant phenotype on the right side of the brain, we could not detect obvious asymmetry in *cachd1*/Cachd1 expression until long after habenula asymmetry had been established (fig. S8). Early Nodal signaling-dependent brain (*28, 29*) and visceral (*30*) asymmetries were unperturbed in *cachd1* mutant embryos (fig. S9). These results suggest that *cachd1* functions locally within the progenitor domain that gives rise to habenula neurons.

Cachd1 functions in both habenulae to promote right-sided and/or suppress left-sided character

Asymmetries in dHb gene expression, synaptic neuropil and targeting of neuronal connections (*5, 8-10, 31*) were all reduced in *cachd1* mutants so that the right habenula closely resembled the left (Fig. 2, A to D, and fig. S10). The dHb contain two major subtypes of projection neuron present in different frequencies on right and left (*9, 10, 31*). On the left, dHb_L neurons projecting to the dorsal interpeduncular nucleus (dIPN) predominate, whereas on the right, dHb_M neurons projecting to the ventral IPN (vIPN) are predominant. Unlike in wild-types, in *cachd1*^{u761} mutants the right dHb extensively innervated the dIPN, which is consistent with a higher proportion of right-sided dHb neurons adopting dHb_L character (Fig. 2, A to D). These results show that on the right side of the brain, Cachd1 promotes dHb_M and/or suppresses dHb_L character, but the results do not reveal whether Cachd1 has any function in determining the molecular character of the left habenula.

A small group of parapineal cells is critical for the elaboration of most aspects of left-sided habenula character (*5, 8, 10, 32*). Consequently, if the parapineal is ablated (Fig. 2E) or fails to signal (Fig. 2F, *sox1a*^{ups8} mutant), the left dHb develops with right-sided character. To examine whether the left-sided character of the habenulae in *cachd1* mutants is dependent on parapineal signaling, we ablated the parapineal in *cachd1*^{u761} mutants. As expected, ablation in wild-type siblings led to reduced expression *kctd12.1*, which is normally high on the left (Fig. 2E), and increased expression of *kctd12.2*, which is normally low on the left (Fig. 2E). By contrast, the double-left habenular phenotype of *cachd1* mutants was unaffected by parapineal ablation (Fig. 2E). Similarly, in *cachd1*^{u761}, *sox1a*^{ups8} double mutants, the *cachd1* mutant phenotype was epistatic to the *sox1a* mutant phenotype (Fig. 2F). These results imply that Cachd1 can function on both sides of the brain to suppress left-sided character and/or promote right-sided character. As a corollary to this, it also implies that the signaling role of the parapineal is to antagonize the function of Cachd1 within the left habenula.

Both timing of neurogenesis and the environment into which habenula neurons are born influence their subtype identity (*19, 27*). Previous work has shown that dHb$_L$ neurons tend to be generated earlier than dHb$_M$ neurons, and habenular neurogenesis is initiated earlier on the left than on the right (*27, 28*). Furthermore, early-born neurons on the left have a higher probability of adopting dHb$_L$ character than those on the right (*19, 28*). To elucidate how Cachd1 affects asymmetries in neurogenesis, we performed birth dating experiments to assess both the extent of habenular neurogenesis and timing of birth of *Et(gata2a:EGFP)pku588*-expressing dHb$_L$ neurons (*pku588Et*) (Fig. 2, G to K). Neurogenesis began earlier in *cachd1*^{u761} mutants compared to wild-types, was symmetric on left and right (Fig. 2, H and I, and fig. S11) and diminished over time (Fig. 2J and fig. S11). In addition, early-born neurons in the right habenula of *cachd1* mutants had a higher likelihood of taking on dHb$_L$ character than in wild-types (Fig. 2K and figs. S11 and S12). Cell transplantation experiments showed that as expected for a protein expressed in dividing cells, Cachd1 does not have strictly cell-autonomous consequences on selection of subtype identity (fig. S13).

Cachd1 binds to Wnt pathway receptors

Given that the biochemical function of Cachd1 was unknown, we performed an unbiased screen to find partners that could interact with the extracellular domain of Cachd1. We identified FZD7 as a potential binding partner in a Retrogenix Cell Microarray Technology screen using a human CACHD1 ectodomain (ECD) multimer as prey protein (fig. S14). To validate the interaction, we tested binding of FLAG-tagged CACHD1 to live, intact human embryonic kidney (HEK) 293E cells expressing full-length, EGFP-tagged FZD7 (FZD7-EGFP) by means of flow cytometry. We observed a strong shift of anti-FLAG phycoerythrin-conjugate (PE) fluorescence in EGFP-positive cells tested with CACHD1 prey, but not an unrelated prey protein (Fig. 3, A and B, and fig. S14). Binding was greatly reduced by preincubation with OMP-18R5, a monoclonal antibody to human FZD7 that binds an epitope in the extracellular, N-terminal cysteine-rich-domain (CRD) of several related FZD receptors (Fig. 3A and fig. S15) (*33*). This suggests that the N-terminal domain of FZD7 contains the binding site for CACHD1.

Because the CRD is very similar between Fzd proteins, using flow cytometry we tested most zebrafish Frizzled family members for binding to Cachd1 (Fig. 3B and fig. S14). Cachd1 prey bound to cells transfected with EGFP fusion constructs of both zebrafish Fzd7 orthologues and most other Frizzled family members tested. Interactions with Fzd1, Fzd2,

Fzd7a and Fzd7b were also effectively inhibited by pre-incubation with OMP-18R5 (fig. S15). Furthermore, human CACHD1 prey protein was able to bind zebrafish Frizzled proteins and vice versa (fig. S14), suggesting strong conservation of interactions.

We used surface plasmon resonance (SPR) to measure binding affinity between purified recombinant mammalian CACHD1 and FZD orthologues. Purified mouse CACHD1 extracellular domain analyte ($CACHD1_{ECD}$) interacted with immobilized human $FZD7_{CRD}$, albeit with low affinity [equilibrium dissociation constant (K_D) = 14.17 ± 2.18 μM] (Fig. 3C and fig. S16), and with mouse $FZD5_{CRD}$ and human $FZD8_{CRD}$ with much higher affinity (K_D = 0.48 ± 0.04 μM and 0.95 ± 0.06 μM respectively) (Fig. 3C and fig. S16).

Wnt ligands use FZDs and LRP5/6 receptors to initiate Wnt signaling (*23*). To test whether CACHD1 could also interact with LRP6, we used immobilized human, membrane distal ($LRP6_{P1E1P2E2}$) and membrane proximal ($LRP6_{P3E3P4E4}$) fragments in SPR. $CACHD1_{ECD}$ interacted with high affinity with the $LRP6_{P3E3P4E4}$ fragment (K_D = 0.17 ± 0.01 μM) (Fig. 3C and fig. S16) and with low affinity with $LRP6_{P1E1P2E2}$ (K_D = 5.86 ± 0.62 μM) (fig. S16).

To test whether binding of CACHD1 to canonical Wnt receptors affected signaling, we performed TOPFlash assays in HEK293 cells (Fig. 3D) (*34*). The response to WNT3A treatment was reduced in cells transfected with full-length *Cachd1* or its ectodomain, but not with the intracellular domain. Furthermore, sensitivity of HEK293 cells to Wnt ligand in the presence of RSPONDIN1 (*35*) was reduced approximately 89% in cells transfected with *cachd1* (fig. S17). The effect of *cachd1* transfection on canonical Wnt signaling differed between colorectal cancer cell lines, suggesting biological context-dependent regulation of Wnt signaling (fig. S17).

Structural characterization of CACHD1 complex with FZD5 and LRP6

Guided by our in vitro measurements, we attempted cocrystallization of $CACHD1_{ECD}$ with $FZD5_{CRD}$ and $LRP6_{P3E3P4E4}$. Resultant crystals diffracted to 4.7Å resolution. The structure was determined with molecular replacement by using crystal structures of the $CACHD1_{ECD}$:$FZD5_{CRD}$ complex, previously determined in our laboratory [Protein Data Bank (PDB) ID 9EQ6], and $LRP6_{P3E3P4E4}$ (PDB ID 4A0P) (*36*). There are three ternary complexes in an asymmetric unit (ASU). Refinement yielded complete structures of equivalent quality for all three copies (table S2), of which one representative complex is depicted in Fig. 4A (PDB ID 8S7C). As expected, $CACHD1_{ECD}$ shows overall structural similarity to the α2δ1 auxiliary subunits of the voltage-gated Ca^{2+} channel Cav1.1 (PDB ID 5GJV; 778 Cα aligned at root mean square deviation = 4.4 Å) (*37*-*39*), which contain two dCache domains and a VWA domain. However, the CACHD1 structure reveals an addition to the C-terminal region of the ECD that does not show any homology to known structures in PDB by Dali search (*40*). This region interfaces with $FZD5_{CRD}$ (Fig. 4A) and we therefore term it the FZD interaction (FZI) domain. The two α helices of the N-terminal dCache domain (C-1) interact with the $LRP6_{P3}$ propeller (Fig. 4A). Thus, CACHD1 serves as a cross-linking component in the ternary complex, independently binding to $FZD5_{CRD}$ and $LRP6_{P3E3P4E4}$.

Structural superpositions show that the CACHD1 binding site on $FZD5_{CRD}$ overlaps with the "thumb" and palmitoleic acid (PAM) lipid binding site (*41*, *42*) required for the receptor-ligand interaction with Wnt (Fig. 4B). Functional studies have indicated that $LRP6_{P3E3P4E4}$ harbors the primary binding site for WNT3A (*43*) and also for the C-terminal domain of DKK-1 (DKK-1C), an inhibitor that competes with Wnts for binding to LRP5/6 (*23*). Crystal structures of $LRP6_{P3E3P4E4}$:DKK-1 complexes (PDB IDs 3S2K, 3S8V and 5FWW) detail the

interaction of the DKK-1 C-terminal domain with $LRP6_{P3}$ (*44-46*). Superposition of our $LRP6_{P3E3P4E4}$:$CACHD1_{ECD}$ structure with the $LRP6_{P3E3P4E4}$:DKK-1C complex (PDB ID 5FWW) shows a steric clash between the CACHD1 C-1 helices and DKK-1C (Fig. 4C). This suggests that CACHD1 may also compete with WNT3A for binding to the $LRP6_{P3}$ propeller (*43*). These biophysical and structural analyses suggest that CACHD1 binds members both of the FZD family and the LRP6 Wnt co-receptors.

cachd1 genetically interacts with Wnt pathway genes

If Cachd1 functions with Fzd and Lrp6 proteins during habenular development, then abrogation of Fzd and/or Lrp6 function may also result in habenular asymmetry phenotypes. The Fzd family is large (*23*), so we focused analysis on Lrp6 function in habenular development. We generated several predicted *lrp6* null alleles and found that homozygous mutants showed a fully penetrant, symmetrical double-left habenular phenotype (Fig. 5A, fig. S18 and table S3). We tested for a genetic interaction between *cachd1* and *lrp6* by injecting a *cachd1* splice-blocking morpholino into heterozygous $lrp6^{u349/+}$ embryos at a low dose that rarely leads to symmetric habenulae in wild-types. We observed that heterozygous $lrp6^{u349/+}$ larvae were approximately three times more likely to show bilaterally symmetric habenular *kctd12.1* expression than wildtype siblings (Fig. 5B). Confirming that this difference was not due to morpholino efficacy, injection of a standard dose caused bilateral symmetry in both genotypes (Fig. 5B). Because these results suggest Cachd1 and Lrp6 function in the same developmental pathway, we next assessed genetic interactions between *cachd1* and two other Wnt pathway genes implicated in habenular development: *axin1* and *tcf7l2* (*18, 19*).

Tcf7l2 is a transcriptional effector of Wnt signaling and loss of *tcf7l2* function results in symmetric habenulae with double-left character (*19*). $tcf7l2^{zf55/+}$ heterozygotes show a wild-type habenular phenotype, but when *cachd1* expression was reduced in $tcf7l2^{zf55/+}$ heterozygotes through injection of low dose *cachd1* morpholino, many larvae showed symmetric, double-left habenulae (Fig. 5C). Consequently, reduced activity of both genes results in a phenotype comparable with that seen when either alone is fully abrogated.

Compromised function of the β-catenin degradation complex scaffolding protein Axin1 results in symmetric habenulae with double-right character (*18*), in contrast to the phenotype of *cachd1* mutants. $axin1^{tm213}$, $cachd1^{u761}$ double mutants exhibited the *axin1* mutant phenotype (as assessed by expression of *kctd12.1*) (Fig. 5D). Consequently, compromised Axin1 function is epistatic to loss of Cachd1 function, consistent with Axin1 functioning downstream of Cachd1 and the Fzd/Lrp6 receptor complex.

Wnt signaling often regulates expression of Wnt-pathway genes (*23*), and the spatially localized expression of *cachd1* along the dorsal forebrain is similar to that of other Wnt pathway genes such as *wnt1*, *wnt3a*, *wnt10b* (*47*), *axin2* and *lef1* (fig. S19). To test whether CACHD1 is itself a target of Wnt signaling, we used quantitative reverse transcription polymerase chain reaction (RT-qPCR) to assess CACHD1 expression in HEK293 cells under different conditions: treatment with WNT3A-conditioned media, treatment with WNT3A+RSPONDIN1-conditioned media, and carrying a stable mutation in *APC* (*48*). Moreover, we performed the same experiment in mouse *Apc*-mutant organoids. *CACHD1*/*Cachd1* showed similar transcriptional responses to enhanced Wnt pathway activity as other Wnt target genes (Fig. 5, E and F), whereas *CACHD1* expression was reduced in cells derived from colorectal cancers (Fig. 5G). Complementarily, global

overexpression of *cachd1* in vivo caused a reduction in expression of the Wnt target *axin2* (fig. S20).

These results provide compelling evidence that the structural interactions we have demonstrated are pertinent to Cachd1 function in the developing brain.

Discussion:

Our studies identify Cachd1 as a component of the Wnt pathway that bridges Fzd and Lrp6 Wnt receptors and plays an important role in the developing zebrafish brain. Recent studies in mice and humans suggest CACHD1 may function in other contexts involving Wnt pathway activity (*49, 50*). We demonstrate evolutionary conserved interactions between CACHD1 and multiple FZD receptors through a previously unidentified FZI domain that could potentially compete with Wnts binding to FZDs through their PAM moiety. Similarly, binding of the dCache domain of CACHD1 to LRP6 may compete with Wnts and the Wnt inhibitor, DKK-1.

The simultaneous binding of Cachd1 to Fzd and Lrp6 receptors could potentially activate signaling by clustering the cytoplasmic apparatus as observed with artificial ligands (*51*). This would be consistent with the similarity of habenular phenotypes in *cachd1*, *lrp6* and *tcf7l2* (*19*) mutants and contrast the phenotype of *axin1* mutants in which the pathway is overactivated (*18*). However, in vitro reporter assays show that Cachd1 can inhibit Wnt signaling and we remain circumspect about the consequences of Cachd1 function in the developing habenulae given the complexity of events in vivo.

Our study suggests that asymmetric Cachd1-dependent modulation of Wnt signaling leads to lateralization of habenula neurons by altering both timing of neurogenesis and the probabilistic selection between alternate neuronal fates. We show that Cachd1 is present and can function on both sides of the brain, but its activity on the left is antagonized by an unknown signal (or signals) from the parapineal. During habenular development, as in many other contexts, Wnt signaling functions at multiple stages and in multiple processes, from proliferation to acquisition and maintenance of cell identity [this study and (*18-21*)]. It is largely unclear how this complexity of pathway activity and outcome is effected, and an attractive possibility is that context-dependent activity of Cachd1 may contribute to this poorly understood aspect of Wnt signaling.

References and Notes:

1. M. L. Concha, I. H. Bianco, S. W. Wilson, Encoding asymmetry within neural circuits. *Nat Rev Neurosci* **13**, 832-843 (2012).
2. L. J. Rogers, G. Vallortigara, Brain and behavioural asymmetries in non-human species. *Laterality* **26**, v-vii (2021).
3. G. Vallortigara, L. J. Rogers, A function for the bicameral mind. *Cortex* **124**, 274-285 (2020).
4. G. Vallortigara, L. J. Rogers, Survival with an asymmetrical brain: advantages and disadvantages of cerebral lateralization. *Behav Brain Sci* **28**, 575-589; discussion 589-633 (2005).
5. M. L. Concha *et al.*, Local tissue interactions across the dorsal midline of the forebrain establish CNS laterality. *Neuron* **39**, 423-438 (2003).
6. M. L. Concha, S. W. Wilson, Asymmetry in the epithalamus of vertebrates. *J Anat* **199**, 63-84 (2001).

7. I. H. Bianco, S. W. Wilson, The habenular nuclei: a conserved asymmetric relay station in the vertebrate brain. *Philos Trans R Soc Lond B Biol Sci* **364**, 1005-1020 (2009).
8. J. T. Gamse, C. Thisse, B. Thisse, M. E. Halpern, The parapineal mediates left-right asymmetry in the zebrafish diencephalon. *Development* **130**, 1059-1068 (2003).
9. H. Aizawa *et al.*, Laterotopic representation of left-right information onto the dorso-ventral axis of a zebrafish midbrain target nucleus. *Curr Biol* **15**, 238-243 (2005).
10. I. H. Bianco, M. Carl, C. Russell, J. D. Clarke, S. W. Wilson, Brain asymmetry is encoded at the level of axon terminal morphology. *Neural Dev* **3**, 9 (2008).
11. K. J. Turner *et al.*, Afferent Connectivity of the Zebrafish Habenulae. *Front Neural Circuits* **10**, 30 (2016).
12. N. Miyasaka *et al.*, From the olfactory bulb to higher brain centers: genetic visualization of secondary olfactory pathways in zebrafish. *J Neurosci* **29**, 4756-4767 (2009).
13. E. Dreosti, N. Vendrell Llopis, M. Carl, E. Yaksi, S. W. Wilson, Left-right asymmetry is required for the habenulae to respond to both visual and olfactory stimuli. *Curr Biol* **24**, 440-445 (2014).
14. M. E. Miletto Petrazzini, V. A. Sovrano, G. Vallortigara, A. Messina, Brain and Behavioral Asymmetry: A Lesson From Fish. *Front Neuroanat* **14**, 11 (2020).
15. V. Duboc, P. Dufourcq, P. Blader, M. Roussigne, Asymmetry of the Brain: Development and Implications. *Annu Rev Genet* **49**, 647-672 (2015).
16. S. Roberson, M. E. Halpern, Convergence of signaling pathways underlying habenular formation and axonal outgrowth in zebrafish. *Development* **144**, 2652-2662 (2017).
17. M. Roussigne, P. Blader, S. W. Wilson, Breaking symmetry: the zebrafish as a model for understanding left-right asymmetry in the developing brain. *Dev Neurobiol* **72**, 269-281 (2012).
18. M. Carl *et al.*, Wnt/Axin1/beta-catenin signaling regulates asymmetric nodal activation, elaboration, and concordance of CNS asymmetries. *Neuron* **55**, 393-405 (2007).
19. U. Husken *et al.*, Tcf7l2 is required for left-right asymmetric differentiation of habenular neurons. *Curr Biol* **24**, 2217-2227 (2014).
20. Y. S. Kuan *et al.*, Distinct requirements for Wntless in habenular development. *Dev Biol* **406**, 117-128 (2015).
21. L. Guglielmi *et al.*, Temporal control of Wnt signaling is required for habenular neuron diversity and brain asymmetry. *Development* **147**, dev182865 (2020).
22. R. Nusse, H. Clevers, Wnt/beta-Catenin Signaling, Disease, and Emerging Therapeutic Modalities. *Cell* **169**, 985-999 (2017).
23. Z. Steinhart, S. Angers, Wnt signaling in development and tissue homeostasis. *Development* **145**, dev146589 (2018).
24. D. Brafman, K. Willert, Wnt/beta-catenin signaling during early vertebrate neural development. *Dev Neurobiol* **77**, 1239-1259 (2017).
25. E. Y. Rim, H. Clevers, R. Nusse, The Wnt Pathway: From Signaling Mechanisms to Synthetic Modulators. *Annu Rev Biochem* **91**, 571-598 (2022).
26. B. J. Dean, B. Erdogan, J. T. Gamse, S. Y. Wu, Dbx1b defines the dorsal habenular progenitor domain in the zebrafish epithalamus. *Neural Dev* **9**, 20 (2014).
27. H. Aizawa, M. Goto, T. Sato, H. Okamoto, Temporally regulated asymmetric neurogenesis causes left-right difference in the zebrafish habenular structures. *Dev Cell* **12**, 87-98 (2007).
28. M. Roussigne, I. H. Bianco, S. W. Wilson, P. Blader, Nodal signalling imposes left-right asymmetry upon neurogenesis in the habenular nuclei. *Development* **136**, 1549-1557 (2009).

29. M. L. Concha, R. D. Burdine, C. Russell, A. F. Schier, S. W. Wilson, A nodal signaling pathway regulates the laterality of neuroanatomical asymmetries in the zebrafish forebrain. *Neuron* **28**, 399-409 (2000).
30. A. F. Schier, Nodal signaling in vertebrate development. *Annu Rev Cell Dev Biol* **19**, 589-621 (2003).
31. J. T. Gamse *et al.*, Directional asymmetry of the zebrafish epithalamus guides dorsoventral innervation of the midbrain target. *Development* **132**, 4869-4881 (2005).
32. I. Lekk *et al.*, Sox1a mediates the ability of the parapineal to impart habenular left-right asymmetry. *Elife* **8**, e47376 (2019).
33. A. Gurney *et al.*, Wnt pathway inhibition via the targeting of Frizzled receptors results in decreased growth and tumorigenicity of human tumors. *Proc Natl Acad Sci U S A* **109**, 11717-11722 (2012).
34. M. T. Veeman, D. C. Slusarski, A. Kaykas, S. H. Louie, R. T. Moon, Zebrafish prickle, a modulator of noncanonical Wnt/Fz signaling, regulates gastrulation movements. *Curr Biol* **13**, 680-685 (2003).
35. W. de Lau *et al.*, Lgr5 homologues associate with Wnt receptors and mediate R-spondin signalling. *Nature* **476**, 293-297 (2011).
36. S. Chen *et al.*, Structural and functional studies of LRP6 ectodomain reveal a platform for Wnt signaling. *Dev Cell* **21**, 848-861 (2011).
37. J. Wu *et al.*, Structure of the voltage-gated calcium channel Ca(v)1.1 at 3.6 A resolution. *Nature* **537**, 191-196 (2016).
38. S. Dahimene *et al.*, The alpha2delta-like Protein Cachd1 Increases N-type Calcium Currents and Cell Surface Expression and Competes with alpha2delta-1. *Cell Rep* **25**, 1610-1621 e1615 (2018).
39. G. S. Cottrell *et al.*, CACHD1 is an alpha2delta-Like Protein That Modulates CaV3 Voltage-Gated Calcium Channel Activity. *J Neurosci* **38**, 9186-9201 (2018).
40. L. Holm, Using Dali for Protein Structure Comparison. *Methods Mol Biol* **2112**, 29-42 (2020).
41. H. Hirai, K. Matoba, E. Mihara, T. Arimori, J. Takagi, Crystal structure of a mammalian Wnt-frizzled complex. *Nat Struct Mol Biol* **26**, 372-379 (2019).
42. C. Y. Janda, D. Waghray, A. M. Levin, C. Thomas, K. C. Garcia, Structural basis of Wnt recognition by Frizzled. *Science* **337**, 59-64 (2012).
43. E. Bourhis *et al.*, Reconstitution of a frizzled8.Wnt3a.LRP6 signaling complex reveals multiple Wnt and Dkk1 binding sites on LRP6. *J Biol Chem* **285**, 9172-9179 (2010).
44. V. E. Ahn *et al.*, Structural basis of Wnt signaling inhibition by Dickkopf binding to LRP5/6. *Dev Cell* **21**, 862-873 (2011).
45. Z. Cheng *et al.*, Crystal structures of the extracellular domain of LRP6 and its complex with DKK1. *Nat Struct Mol Biol* **18**, 1204-1210 (2011).
46. M. Zebisch, V. A. Jackson, Y. Zhao, E. Y. Jones, Structure of the Dual-Mode Wnt Regulator Kremen1 and Insight into Ternary Complex Formation with LRP6 and Dickkopf. *Structure* **24**, 1599-1605 (2016).
47. R. N. Duncan, S. Panahi, T. Piotrowski, R. I. Dorsky, Identification of Wnt Genes Expressed in Neural Progenitor Zones during Zebrafish Brain Development. *PLoS One* **10**, e0145810 (2015).
48. L. Novellasdemunt *et al.*, USP7 Is a Tumor-Specific WNT Activator for APC-Mutated Colorectal Cancer by Mediating beta-Catenin Deubiquitination. *Cell Rep* **21**, 612-627 (2017).

49. E. A. Rutledge, J. D. Benazet, A. P. McMahon, Cellular heterogeneity in the ureteric progenitor niche and distinct profiles of branching morphogenesis in organ development. *Development* **144**, 3177-3188 (2017).
50. M. Scala *et al.*, Biallelic loss-of-function variants in CACHD1 cause a novel neurodevelopmental syndrome with facial dysmorphism and multisystem congenital abnormalities. *Genet Med* **26**, 101057 (2023).
51. C. Y. Janda *et al.*, Surrogate Wnt agonists that phenocopy canonical Wnt and beta-catenin signalling. *Nature* **545**, 234-237 (2017).
52. P. Alestrom *et al.*, Zebrafish: Housing and husbandry recommendations. *Lab Anim* **54**, 213-224 (2020).
53. R. N. Kettleborough *et al.*, A systematic genome-wide analysis of zebrafish protein-coding gene function. *Nature* **496**, 494-497 (2013).
54. C. P. Heisenberg *et al.*, A mutation in the Gsk3-binding domain of zebrafish Masterblind/Axin1 leads to a fate transformation of telencephalon and eyes to diencephalon. *Genes Dev* **15**, 1427-1434 (2001).
55. V. Muncan *et al.*, T-cell factor 4 (Tcf7l2) maintains proliferative compartments in zebrafish intestine. *EMBO Rep* **8**, 966-973 (2007).
56. D. T. Gilmour, H. M. Maischein, C. Nusslein-Volhard, Migration and function of a glial subtype in the vertebrate peripheral nervous system. *Neuron* **34**, 577-588 (2002).
57. L. Wen *et al.*, Visualization of monoaminergic neurons and neurotoxicity of MPTP in live transgenic zebrafish. *Dev Biol* **314**, 84-92 (2008).
58. F. J. van Eeden, M. Granato, J. Odenthal, P. Haffter, Developmental mutant screens in the zebrafish. *Methods Cell Biol* **60**, 21-41 (1999).
59. J. C. Talbot, S. L. Amacher, A streamlined CRISPR pipeline to reliably generate zebrafish frameshifting alleles. *Zebrafish* **11**, 583-585 (2014).
60. F. Kroll *et al.*, A simple and effective F0 knockout method for rapid screening of behaviour and other complex phenotypes. *Elife* **10**, e59683 (2021).
61. W. S. Talbot, A. F. Schier, Positional cloning of mutated zebrafish genes. *Methods Cell Biol* **60**, 259-286 (1999).
62. R. H. Row, D. Kimelman, Bmp inhibition is necessary for post-gastrulation patterning and morphogenesis of the zebrafish tailbud. *Dev Biol* **329**, 55-63 (2009).
63. K. M. Bushell, C. Sollner, B. Schuster-Boeckler, A. Bateman, G. J. Wright, Large-scale screening for novel low-affinity extracellular protein interactions. *Genome Res* **18**, 622-630 (2008).
64. G. Lennon, C. Auffray, M. Polymeropoulos, M. B. Soares, The I.M.A.G.E. Consortium: an integrated molecular analysis of genomes and their expression. *Genomics* **33**, 151-152 (1996).
65. C. Sollner, G. J. Wright, A cell surface interaction network of neural leucine-rich repeat receptors. *Genome Biol* **10**, R99 (2009).
66. Y. Zhao, J. Ren, S. Padilla-Parra, E. E. Fry, D. I. Stuart, Lysosome sorting of beta-glucocerebrosidase by LIMP-2 is targeted by the mannose 6-phosphate receptor. *Nat Commun* **5**, 4321 (2014).
67. Y. Durocher, S. Perret, A. Kamen, High-level and high-throughput recombinant protein production by transient transfection of suspension-growing human 293-EBNA1 cells. *Nucleic Acids Res* **30**, E9 (2002).
68. M. Loignon *et al.*, Stable high volumetric production of glycosylated human recombinant IFNalpha2b in HEK293 cells. *BMC Biotechnol* **8**, 65 (2008).

69. P. J. Reeves, N. Callewaert, R. Contreras, H. G. Khorana, Structure and function in rhodopsin: high-level expression of rhodopsin with restricted and homogeneous N-glycosylation by a tetracycline-inducible N-acetylglucosaminyltransferase I-negative HEK293S stable mammalian cell line. *Proc Natl Acad Sci U S A* **99**, 13419-13424 (2002).
70. T. Sato *et al.*, Single Lgr5 stem cells build crypt-villus structures in vitro without a mesenchymal niche. *Nature* **459**, 262-265 (2009).
71. J. Freeth, J. Soden, New Advances in Cell Microarray Technology to Expand Applications in Target Deconvolution and Off-Target Screening. *SLAS Discov* **25**, 223-230 (2020).
72. L. Turner *et al.*, Severe malaria is associated with parasite binding to endothelial protein C receptor. *Nature* **498**, 502-505 (2013).
73. A. R. Aricescu, W. Lu, E. Y. Jones, A time- and cost-efficient system for high-level protein production in mammalian cells. *Acta Crystallogr D Biol Crystallogr* **62**, 1243-1250 (2006).
74. T. C. Terwilliger *et al.*, Iterative model building, structure refinement and density modification with the PHENIX AutoBuild wizard. *Acta Crystallogr D Biol Crystallogr* **64**, 61-69 (2008).
75. C. Thisse, B. Thisse, High-resolution in situ hybridization to whole-mount zebrafish embryos. *Nat Protoc* **3**, 59-69 (2008).
76. H. M. Choi *et al.*, Mapping a multiplexed zoo of mRNA expression. *Development* **143**, 3632-3637 (2016).
77. K. J. Turner, T. G. Bracewell, T. A. Hawkins, Anatomical dissection of zebrafish brain development. *Methods Mol Biol* **1082**, 197-214 (2014).
78. G. A. Michael, A significance test of interaction in 2 x K designs with proportions. *TQMP* **3**, 1-7 (2007).
79. N. Percie du Sert *et al.*, The ARRIVE guidelines 2.0: Updated guidelines for reporting animal research. *PLoS Biol* **18**, e3000410 (2020).
80. B. Kilian *et al.*, The role of Ppt/Wnt5 in regulating cell shape and movement during zebrafish gastrulation. *Mech Dev* **120**, 467-476 (2003).
81. S. Witzel, V. Zimyanin, F. Carreira-Barbosa, M. Tada, C. P. Heisenberg, Wnt11 controls cell contact persistence by local accumulation of Frizzled 7 at the plasma membrane. *J Cell Biol* **175**, 791-802 (2006).
82. Z. M. Varga *et al.*, Zebrafish smoothened functions in ventral neural tube specification and axon tract formation. *Development* **128**, 3497-3509 (2001).
83. G. Weidinger, C. J. Thorpe, K. Wuennenberg-Stapleton, J. Ngai, R. T. Moon, The Sp1-related transcription factors sp5 and sp5-like act downstream of Wnt/beta-catenin signaling in mesoderm and neuroectoderm patterning. *Curr Biol* **15**, 489-500 (2005).
84. T. Kudoh *et al.*, A gene expression screen in zebrafish embryogenesis. *Genome Res* **11**, 1979-1987 (2001).
85. F. Biemar *et al.*, Pancreas development in zebrafish: early dispersed appearance of endocrine hormone expressing cells and their convergence to form the definitive islet. *Dev Biol* **230**, 189-203 (2001).
86. S. Long, N. Ahmad, M. Rebagliati, The zebrafish nodal-related gene southpaw is required for visceral and diencephalic left-right asymmetry. *Development* **130**, 2303-2316 (2003).
87. C. Thisse, B. Thisse, Antivin, a novel and divergent member of the TGFbeta superfamily, negatively regulates mesoderm induction. *Development* **126**, 229-240 (1999).

88. G. Lupo *et al.*, Retinoic acid receptor signaling regulates choroid fissure closure through independent mechanisms in the ventral optic cup and periocular mesenchyme. *Proc Natl Acad Sci U S A* **108**, 8698-8703 (2011).
89. S. Krauss, V. Korzh, A. Fjose, T. Johansen, Expression of four zebrafish wnt-related genes during embryogenesis. *Development* **116**, 249-259 (1992).
90. L. E. Valdivia *et al.*, Lef1-dependent Wnt/beta-catenin signalling drives the proliferative engine that maintains tissue homeostasis during lateral line development. *Development* **138**, 3931-3941 (2011).

Acknowledgments: We thank many colleagues for support and advice during the course of this project; staff at Diamond Light Source for assistance with X-ray data collection; Dr Austin Gurney for supplying the OMP-18R5 antibody; Jim Freeth, Mark Aspinall-O'Dea, Karen Williams and Natalia Guardiola at Charles River Discovery Research Services UK Limited for Cell Microarray technology; and the UCL Fish Facility for fish husbandry.

Funding: This research was funded in whole, or in part, by the Wellcome Trust (see below). For the purpose of open access, the authors have applied a CC BY public copyright license to any Author Accepted Manuscript version arising from this submission.

Wellcome Trust Investigator Award (104682/Z/14/Z) to S.W.W.

Wellcome Trust Project Grant (088175/Z/09/Z) to S.W.W. and R.M.Y.

Wellcome Discovery Award (225445/Z/22/Z) to S.W.W. and I. Bianco

MRC Programme Grants (MR/L003775/1 and MR/T020164/1) to S.W.W. and G.G.

Wellcome Trust (223133/Z/21/Z) to E.Y.J.

Cancer Research UK (C375/A17721) to E.Y.J.

MRC award (MR/M000141/1) to E.Y.J.

Wellcome Trust award (206194) to G.J.W.

Wellcome Trust Award (101122/Z/13/Z) to J.R.

The laboratory of V.S.W.L. is supported by the Francis Crick Institute, which receives its core funding from Cancer Research UK (FC001105), the UK Medical Research Council (FC001105) and the Wellcome Trust (FC001105).

Author contributions: The senior authors emphasize that all four lead authors made equally important contributions to this study, and individuals may list the joint authors in whichever order they wish on CVs and other personal documents.

Conceptualization: G.T.P., A.F., Y.Z., H.S., J.R., E.Y.J., S.W.W.

Methodology: G.T.P., A.F., Y.Z., H.S., J.R., W.L., R.M.Y., Q.S., V.S.W.L., G.J.W., E.Y.J., S.W.W.

Validation: G.T.P., A.F., Y.Z., H.S., J.R., V.S.W.L., E.Y.J., S.W.W.

Formal analysis: G.T.P., A.F., Y.Z.

Investigation: G.T.P., A.F., Y.Z., H.S., L.N., P.H., G.G., E.R.W., J.R., W.L., R.M.Y., T.A.H., F.C., Q.S., V.S.W.L.

Resources: G.T.P., A.F., Y.Z., G.G., W.L., T.A.H., F.C., E.D., V.S.W.L., S.W.W.

Data curation: G.T.P., A.F., Y.Z.

Writing – original draft: G.T.P., A.F., Y.Z., E.Y.J., S.W.W.

Writing – review & editing: G.T.P., Y.Z., H.S., D.W.R., E.Y.J., S.W.W.

Visualization: G.T.P., A.F., Y.Z., H.S., V.S.W.L.

Supervision: A.F., H.S., R.M.Y., D.W.R., E.Y.J., S.W.W.

Project administration: E.Y.J., S.W.W.

Funding acquisition: G.G., J.R., R.M.Y., V.S.W.L., G.J.W., E.Y.J., S.W.W.

Competing interests: The authors declare no competing financial interests.

Data and materials availability: The crystal structure of the $CACHD1_{ECD}$:$FZD5_{CRD}$:$LRP6_{P3E3P4E4}$ ternary complex is available at the Research Collaboratory for Structural Bioinformatics Protein Data Bank under accession no. 8S7C.

Further information and requests relating to zebrafish resources and reagents, including mutants generated in this study, should be directed to G.T.P. (g.powell@ucl.ac.uk) and S.W.W. (s.wilson@ucl.ac.uk), information and requests relating to structural biology and biochemistry should be directed to E.Y.J. (yvonne.jones@strubi.ox.ac.uk) and Y.Z. (yuguang.zhao@strubi.ox.ac.uk).

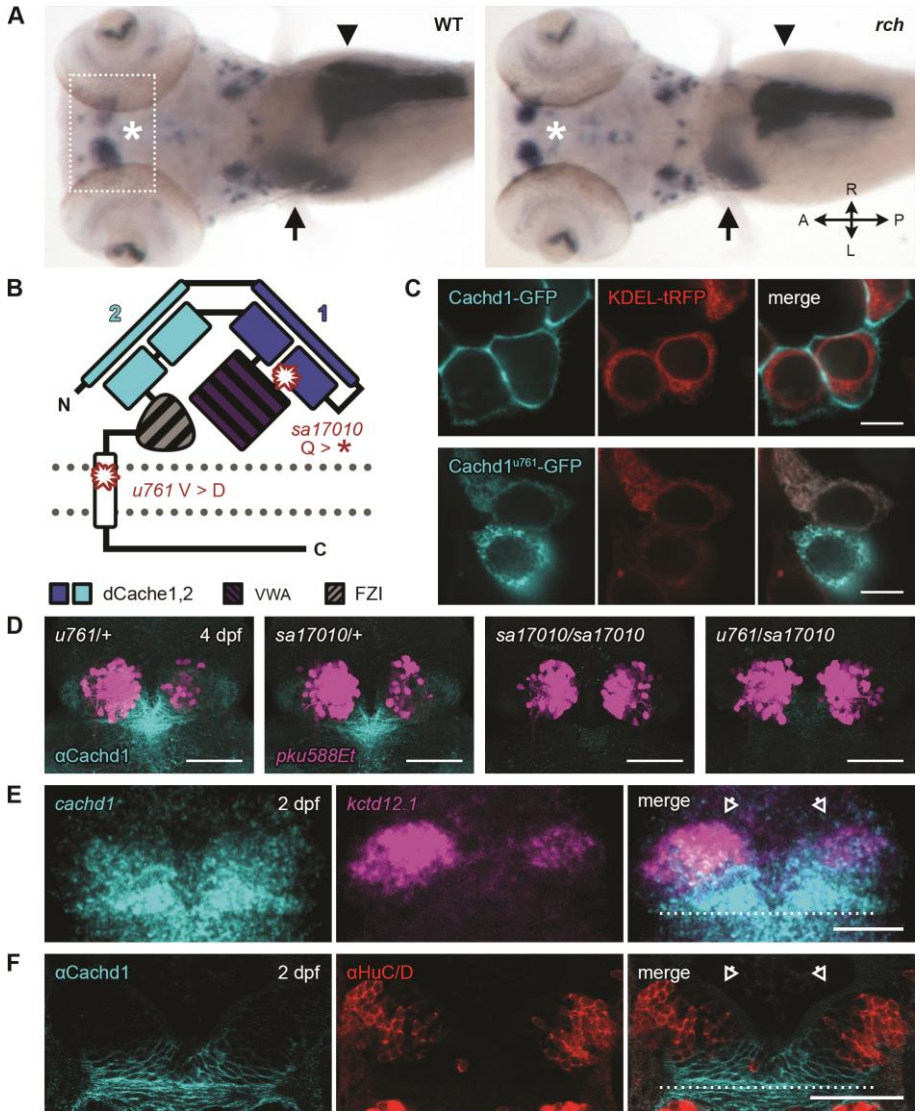

Fig. 1. *cachd1* mutants show bilaterally symmetrical, double-left habenulae.
(**A**) Dorsal views of whole-mount 5 dpf wild-type sibling and *rorschach* (*rch*/*u761*) mutant larvae showing expression of an asymmetric habenular marker (*kctd12.1*, indicated with asterisk; box indicates approximate epithalamic region) and markers for liver (*selenop2*, indicated with arrow), pancreas (*prss1*, indicated with arrowhead), and ventral retina (*aldh1a3*). (**B**) Schematic of Cachd1 protein: two dCache domains (cyan and dark blue), a VWA domain (purple stripes), a FZD interaction domain (FZI; gray stripes), a transmembrane domain (white), and an unstructured cytoplasmic tail. Residues affected in *sa17010* and *u761* alleles are marked in red at approximate positions in primary sequence. (**C**) Fluorescence images of transfected HEK293T cells expressing constructs encoding EGFP-tagged wild-type (top; cyan) or *rch*/*u761* mutant Cachd1 (bottom; cyan) and KDEL-tRFP (red) to mark the endoplasmic reticulum. Scale bar, 10 μm. (**D**) Dorsal views of brains of dissected 4 dpf transgenic siblings from a complementation cross of *sa17010* and *u761* alleles, stained with antibody to Cachd1 (cyan). The *Et(gata2a:EGFP)pku588* (*pku588Et*) transgene is expressed in dHb_L neurons (magenta). (**E**) Dorsal view of 2 dpf habenulae after double fluorescent in situ hybridization with *cachd1* antisense riboprobe (cyan) and the dHb_L marker *kctd12.1* (magenta). (**F**) Dorsal views of 2 dpf habenulae after immunohistochemistry with antibody to Cachd1 (cyan) co-stained with antibody

to HuC/D to mark differentiating neurons (red). The dotted lines in (E) and (F) indicate the approximate position of the posterior commissure; open arrowheads indicate the dorsal habenulae. Shown are maximum projections of [(D) and (E)] confocal z-stacks or (F) single confocal slice. Scale bars, 50 μm.

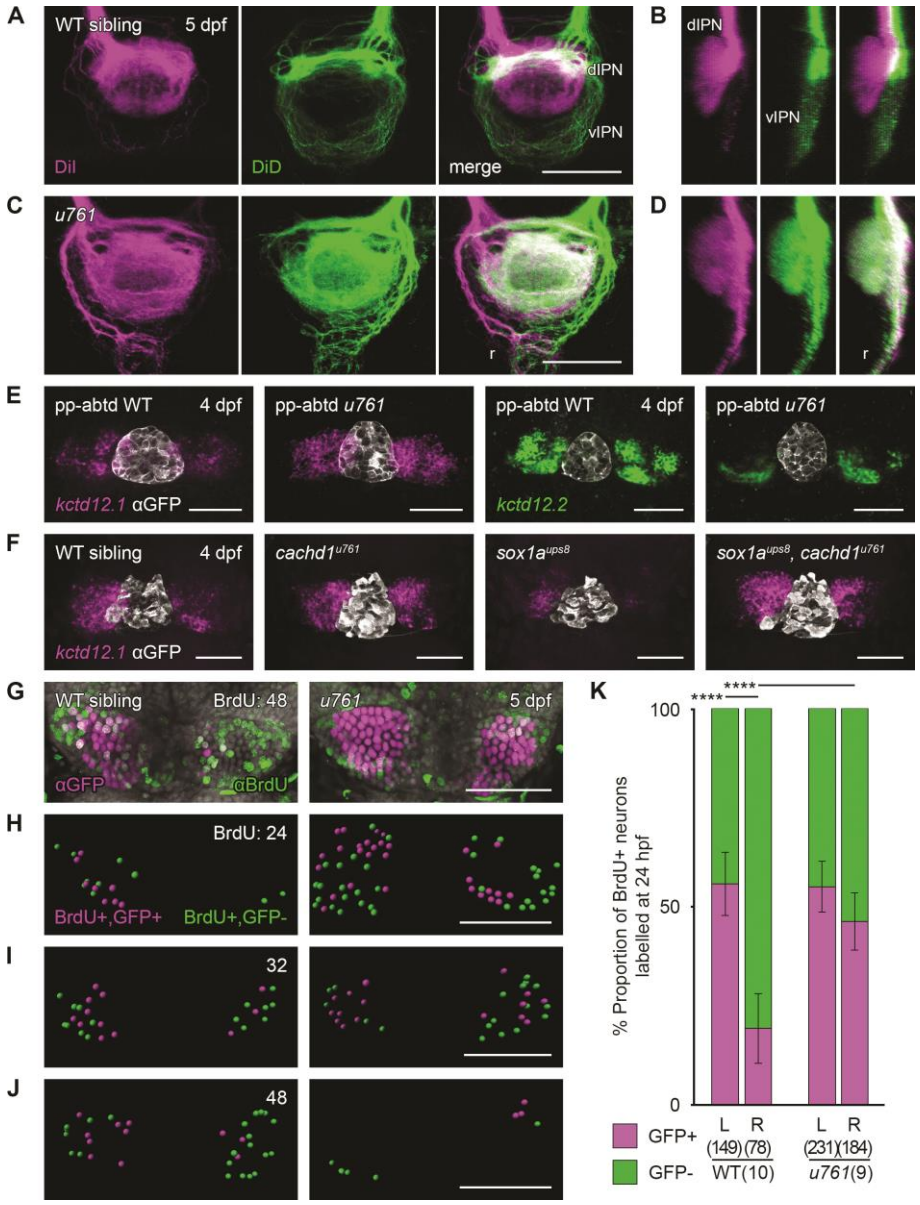

Fig. 2. Loss of function of *cachd1* disrupts habenular efferent connectivity, is epistatic to removal of the parapineal signal, and causes precocious neurogenesis.

(**A** and **C**) Dorsal views and (B and D) sagittal projections (dorsal left) of the IPN showing DiI (magenta) and DiD (green) labelling of left- and right-sided habenula neuron axon terminals predominantly innervating the dIPN and vIPN respectively, and raphe (r), in 5 dpf wild-type [(A) and (B), *n* = 3] or *cachd1*^{u761} mutant [(C) and (D), *n* = 8] larvae. (**E**) Dorsal views of 4 dpf wild-type or *cachd1*^{u761} mutant epithalami in which the parapineal was ablated before leftward migration (pineal complex marked by *zf104Tg*, *u711Tg* alleles with antibody to GFP; white) after double FISH with *kctd12.1* (magenta; *n* = 26 of 29 wild-type siblings, 11 of 12 *cachd1*^{u761} mutants) or *kctd12.2* (green; *n* = 19 of 23 wild-type siblings, 5 of 5 *cachd1*^{u761} mutants). (**F**) Dorsal views of 4 dpf larvae from a cross of carriers of *cachd1*^{u761} and *sox1a*^{ups8} alleles after FISH with *kctd12.1* [magenta; pineal complex as (C), white]. *n* = 4 wild-types, 3 *cachd1*^{u761} mutants, 4 *sox1a*^{ups8} mutants, 3 *sox1a*^{ups8}, *cachd1*^{u761} double mutants. (**G**) Dorsal views of

Et(gata2a:EGFP)pku588 wild-type or *cachd1*^{u761} mutant habenulae incubated at 48 hours post fertilization (hpf) with a pulse of BrdU to label newly born neurons, then processed for immunohistochemistry at 5 dpf with antibody to GFP (magenta) and antibody to BrdU (green). DAPI (4′,6-diamidino-2-phenylindole) counterstain marks nuclei (gray). (**H** to **J**) Segmentation of confocal stacks from *Et(gata2a:EGFP)pku588* wild-type or *cachd1*^{u761} mutant larvae incubated at (H) 24, (I) 32 and (J) 48 hpf with a pulse of BrdU, then processed at 5 dpf as in (G). Double-positive cells are represented in magenta; BrdU-positive only cells are indicated in green. Times of pulse indicated at top right. (**K**) Quantification of the proportion of BrdU-positive neurons that also expressed *Et(gata2a:EGFP)pku588* (magenta) in 5 dpf wild-type or *cachd1*^{u761} larvae incubated with a pulse of BrdU at 24 hpf (all timepoints presented in fig. S11). Error bars represent 95% confidence intervals. Total number of cells and larvae for each genotype indicated in axis label in parentheses. Q′ test of equality of proportions [24 hpf, degrees of freedom (DF) = 3, $\chi^2 = 40.94$, $P = 6.7 \times 10^{-9}$], post hoc pairwise comparisons using a modified Marascuilo procedure with Benjamini-Hochberg correction for multiple testing, **** $P \leq 0.005$. Scale bars, 50 μm in (A) to (H).

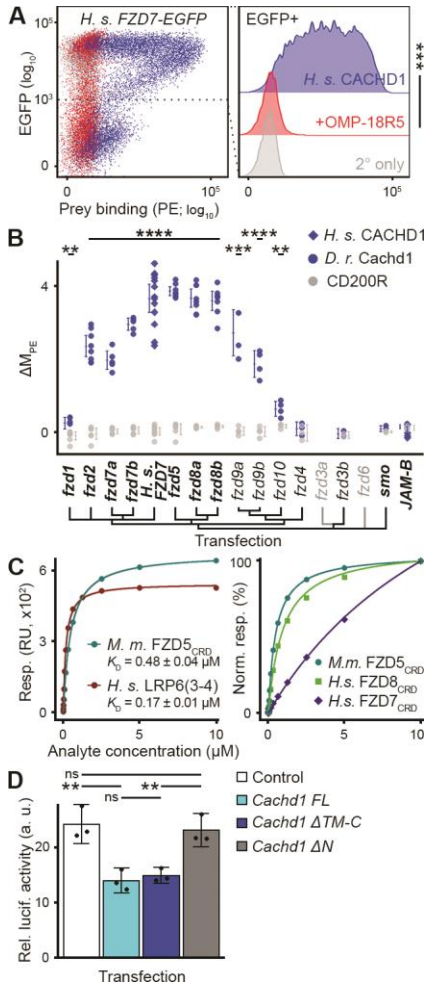

Fig. 3. CACHD1 physically interacts with Wnt receptors LRP6 and FZD family members. (**A**) (Left) Representative scatter plot of flow cytometry testing binding of FLAG-tagged CACHD1 prey protein to human FZD7-EGFP transiently transfected HEK293E cells detected by means of phycoerythrin (PE)-conjugated secondary antibody. (Right) Without (blue) or with (red) preincubation with antibody to Frizzled OMP-18R5; secondary only negative control (gray). $n = 3$; one-tailed paired t test (DF = 2, $t = 9.53$, *** $P = 0.0054$). (**B**) Dot plot of human (blue diamonds) or zebrafish (blue circles) Cachd1 or negative control CD200R (gray) prey protein binding (standardized as ΔM_{PE} (supplementary materials, materials and methods) to cells transiently transfected with EGFP fusion protein constructs indicated (transfections verified by means of antibody labeling are indicated in bold). Each dot indicates a single experiment; horizontal bars indicate the mean, and error bars indicate 95% confidence intervals. One way Welch test of means (Cachd1 prey versus CD200R prey, not assuming equal variances; $F = 132.32$, $DF_{num} = 30.00$, $DF_{denom} = 34.67$, $P = 5.09 \times 10^{-28}$), post hoc pairwise t tests with non-pooled standard deviations, Benjamini-Hochberg correction for multiple testing. Only statistically significant differences between Cachd1 and CD200R prey for individual transfections are presented here for clarity; ** $0.05 \geq P > 0.01$, *** $0.01 \geq P > 0.005$, **** $P \leq 0.005$. (**C**) SPR-based determination of K_D (left) for mouse $CACHD1_{ECD}$ analyte binding to immobilized mouse $FZD5_{CRD}$ (cyan) or human $LRP6_{P3E3P4E4}$ (3-4, red), and normalized response curves (right) for different $CACHD1_{ECD}$:FZD_{CRD} interactions. RU, response units. (**D**) TOPFlash responses of HEK293 cells to WNT3A treatment after transfection with a control plasmid

(white) or plasmids containing full length rodent *Cachd1* (cyan), *Cachd1* extracellular domain only (blue; *ΔTM-C*), or *Cachd1* transmembrane and intracellular domains only (gray; *ΔN*). Mean responses are shown (n = 3 experiments; black dots indicate mean of quadruple technical replicates in each experiment); error bars idicate 95% confidence intervals. One way Welch test of means (not assuming equal variances; F = 13.202, DF_{num} = 3.00, DF_{denom} = 4.19, P = 0.014), post hoc pairwise t tests with non-pooled standard deviations, Benjamini-Hochberg correction for multiple testing. ns, $P > 0.1$, ** $0.05 \geq P > 0.01$.

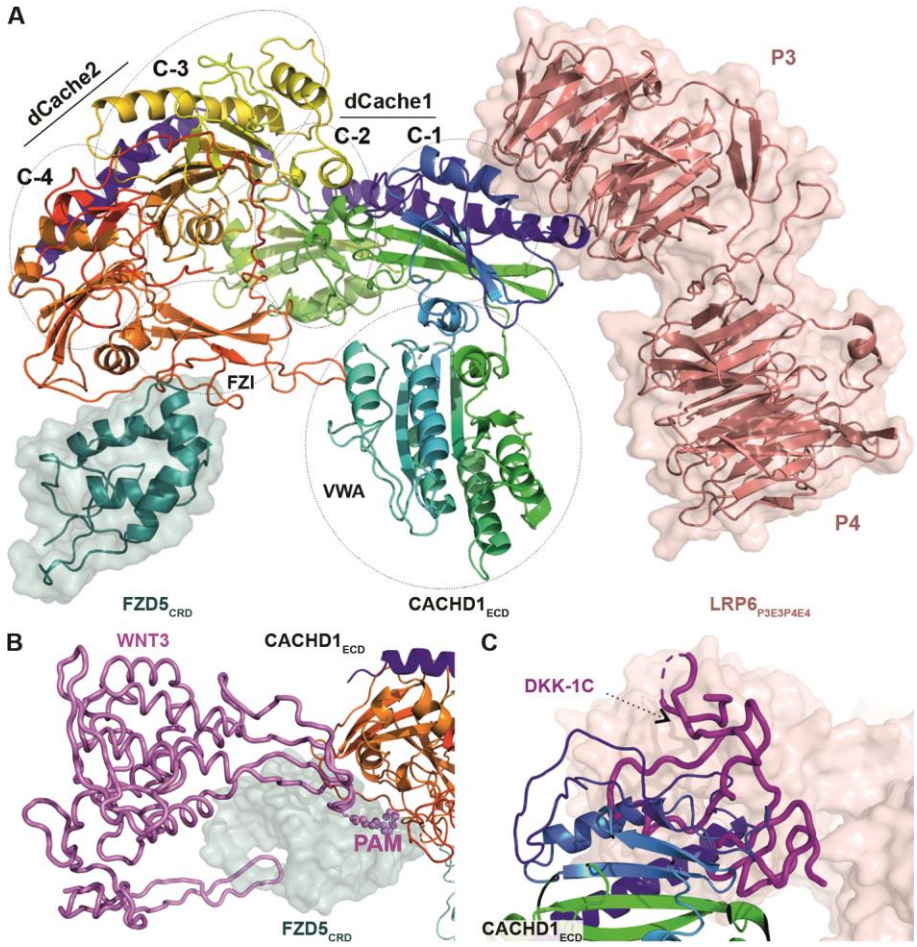

Fig. 4. CACHD1 forms a ternary complex with FZD5 and LRP6.
(**A**) Cartoon representation of mouse $CACHD1_{ECD}$, [rainbow-colored from N terminus (blue) to C terminus (red)] in complex with mouse $FZD5_{CRD}$ (cartoon and surface in teal) and human $LRP6_{P3E3P4E4}$ (cartoon and surface in salmon pink). The position of the four cache (C-1, -2, -3 and -4), VWA and FZD interaction (FZI) domains of $CACHD1_{ECD}$ are indicated (PDB ID 8S7C). (**B**) Superimposed structures of the FZD8:WNT3 complex (PDB ID 6AHY) with the $FZD5_{CRD}$:$CACHD1_{ECD}$ complex. WNT3 is shown as a violet cartoon tube with palmitoleic acid (PAM) as spheres. (**C**) Superimposed structures of the LRP6:DKK1-C complex (PDB ID 5FWW) with the $CACHD1_{ECD}$:$LRP6_{P3E3P4E4}$ complex. DKK1-C is shown as a magenta cartoon tube.

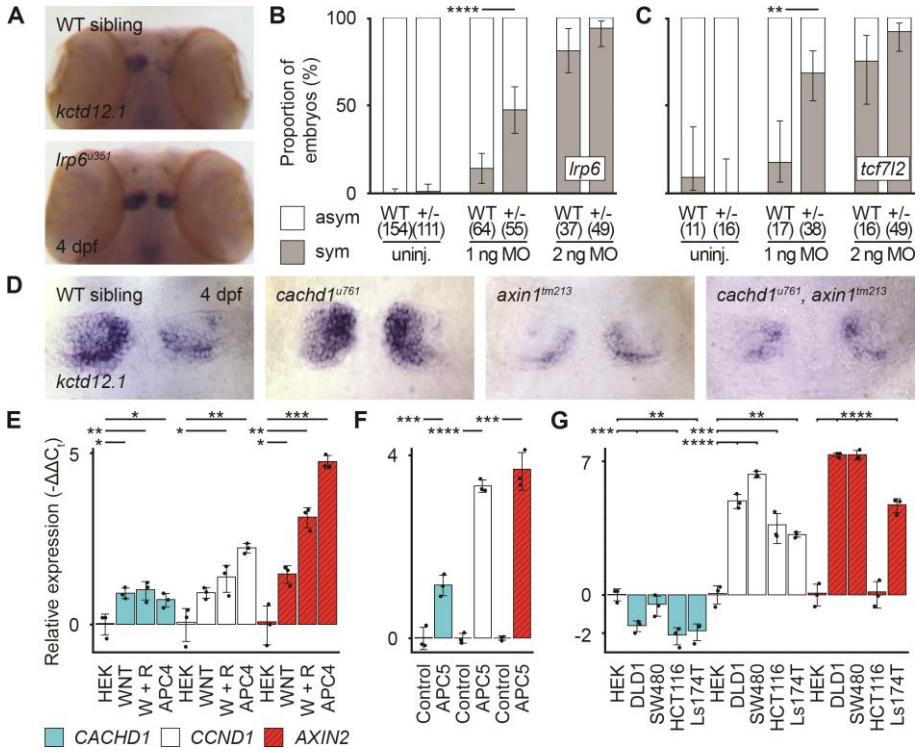

Fig. 5. *cachd1* interacts genetically with Wnt pathway components.
(**A**) Dorsal views of wholemount 4 dpf wild-type sibling (n = 12) and *lrp6*^{u351} mutant (n = 9) heads stained for expression of *kctd12.1*. (**B** and **C**) Graphs showing the percentage of (B) 4 dpf wild-type siblings and *lrp6*$^{u349/+}$ larvae or (C) wild-type siblings and *tcf7l2*$^{zf55/+}$ larvae with (gray; sym) or without (white; asym) a symmetric bilateral left phenotype in uninjected larvae and larvae injected with a suboptimal (1 ng) or standard dose (2 ng) of *cachd1* morpholino (MO1). Error bars indicate 95% confidence intervals of the proportion. Q′ test of equality of proportions [(B) DF = 2, χ^2 = 18.71, P = 8.66 × 10^{-5}; (C) DF = 2, χ^2 = 7.93, P = 0.019) and post hoc modified Marascuilo procedure with Benjamini-Hochberg correction for multiple testing. (**D**) Dorsal views of the habenulae of wholemount 4 dpf larvae from an incross of *cachd1*^{u761} and *axin1*^{tm213} mutants, showing expression of *kctd12.1*. n = 5 wild-types, 6 *cachd1*^{u761} mutants, 3 *axin1*^{tm213} mutants and 3 *cachd1*^{u761}, *axin1*^{tm213} double mutants. (**E** to **G**) Quantitative RT-PCR data showing relative expression (-ΔΔC_t values) of *CACHD1* and known Wnt-responsive genes (*CCND1*, *AXIN2*) in (E) HEK293 (HEK) cells untreated, incubated with WNT3A alone (WNT) or WNT3A and RSPONDIN1-conditioned media (W + R), or stable *APC* mutant cells (*APC4*); (F) wild-type (Control) and *Apc* mutant (*APC5*) mouse organoids; and (G) colorectal cancer-derived cell lines with mutations in Wnt pathway genes (*APC* mutants, DLD1, SW480; *CTNNB1* mutants, HCT116, Ls174T). Data is presented as mean -ΔΔC_t values compared to expression of *ACTB* (human) or *Hrpt1* (mouse) reference genes and untreated controls (HEK293 cells or wild-type organoid). Individual points indicate biological replicates (each an average of three technical replicates), n = 3; error bars indicate 95% confidence intervals. One way Welch test of means [not assuming equal variances; (A) F = 58.83, DF_{num} = 11.00, DF_{denom} = 9.41, P = 3.03 × 10^{-7}; (B) F = 225.66, DF_{num} = 5.00, DF_{denom} = 5.16, P = 5.12 × 10^{-6}; (C) F = 236.49, DF_{num} = 14.00, DF_{denom} = 11.33, P = 7.67 × 10^{-12}], post hoc pairwise t tests with non-pooled standard deviations and Benjamini-Hochberg correction for multiple testing; only statistically significant differences with control samples (HEK or Control) are presented here for clarity. * 0.1 ≥ P > 0.05, ** 0.05 ≥ P > 0.01, *** 0.01 ≥ P > 0.005, **** P ≤ 0.005.

Supplementary Materials for

Cachd1 interacts with Wnt receptors and regulates neuronal asymmetry in the zebrafish brain

Gareth T. Powell[1,2]†, Ana Faro[1]†, Yuguang Zhao[3]*†, Heather Stickney[1,4,5]†, Laura Novellasdemunt[6,7], Pedro Henriques[1], Gaia Gestri[1], Esther Redhouse White[1], Jingshan Ren[3], Weixian Lu[3], Rodrigo M. Young[1,8,9], Thomas A. Hawkins[1], Florencia Cavodeassi[1,10], Quenten Schwarz[8], Elena Dreosti[1], David W. Raible[4], Vivian S. W. Li[6], Gavin J. Wright[2,11], E. Yvonne Jones[3]*, Stephen W. Wilson[1]*

Corresponding authors: Email: s.wilson@ucl.ac.uk (S. W. W.), yvonne.jones@strubi.ox.ac.uk (E. Y. J.), yuguang.zhao@strubi.ox.ac.uk (Y. Z.)

Supplementary Materials contains:

Author contributions:

The senior authors wish to emphasize that all four lead authors made equally important contributions to this study and are happy for individuals to list the joint authors in whichever order they wish on CVs and other documents.

GTP devised and performed experiments (generated/gathered reagents, protein interactions/immunocytochemistry using flow cytometry, immunohistochemistry, *in situ* hybridization chain reaction, *lrp6* mutagenesis, morpholino injections), analyzed data, contributed to writing the paper, prepared figures. AF devised and performed experiments (*in situ* hybridization, immunohistochemistry, BrdU pulse-chase, parapineal ablations, lipophilic dye labelling, epistasis, morpholino injections), analyzed data. YZ devised and performed experiments (structural biology, protein interactions using surface plasmon resonance), analyzed data, prepared figures. HS devised and performed experiments (ENU mutagenesis and screening, genetic mapping, gene identification, morpholino injections, *in situ* hybridization, immunohistochemistry, lipophilic dye labelling, transgenesis and heat shock experiments, tissue culture and transfection), analyzed data. LN devised and performed experiments (qRT-PCR, generated organoids), analyzed data. PH devised and performed experiments (parapineal ablations and *in situ* hybridization), analyzed data. GG designed and performed experiments (phenotype characterization, transplantation). ER-W performed experiments (epistasis and *in situ* hybridization). JR analyzed data (structural phasing/model building). WL generated reagents for research (tissue culture/protein production). RMY, HS, TAH, FC and QS undertook the screen that isolated the *rorschach* mutant. ED generated reagents for research (transgenesis). DWR devised experiments and provided funding for research (supported HS). VWSL provided funding for research (supported LN). GJW

devised experiments and provided funding for research (supported GTP). EYJ provided funding for research (supported YZ, JR, WL), devised experiments, contributed to writing the paper. SWW provided funding for research (supported GTP, AF, HS, PH, ER-W, RMY, TAH, QS, FC, ED), devised experiments, wrote the paper.

Materials and Methods:

Zebrafish husbandry and fish lines

Zebrafish experiments and husbandry followed standard protocols *(52)* in accordance with the UK Home Office (project licenses 70/7071, 70/8449 and PP4300676) or University of Washington Institutional Animal Care and Use Committee guidelines: Office of Laboratory Animal Welfare (OLAW) Assurance Number for the University of Washington D16-00292.

Zebrafish were maintained in designated facilities on a 14h/10h light:dark cycle. Embryos and fry were obtained by natural spawning of wildtype, *cachd1*^{u761} (this study, below), *cachd1*^{sa17010} (Zebrafish Mutation Project; ZFIN: ZDB-ALT-131220-250) *(53)*, *sox1a*^{ups8} (ZDB-FISH-200611-5) *(32)*, *lrp6*^{u348}, *lrp6*^{u349}, *lrp6*^{u350}, *lrp6*^{u351} (this study, below), *axin1*^{tm213} (ZDB-FISH-150901-22104) *(54)*, *tcf7l2*^{zf55} (ZDB-FISH-150901-25729) *(55)*, *Tg(foxd3:GFP)zf104 (56)*, *Tg(-1.6flh:GAP-EGFP)u711* (ZDB-FISH-200530-1) *(5)*, *Et(gata2a:EGFP)pku588* (ZDB-FISH-150901-5098) *(57)*, *Tg(HSE:cachd1, EGFP)w160* (this study, below), *Tg(neurod1:Cachd1-EGFP)w162* (this study, below), *Tg(gng8:EGFP)u775* (this study, below) fish.

Embryos were routinely stored in fish system water supplemented with methylene blue, or E3 embryo medium at 28°C. Where necessary, embryos were treated with 0.2 mM 1-phenyl 2-thiourea (PTU) to prevent pigment formation.

Generation of mutant and transgenic lines

The *u761* mutant was generated by ENU mutagenesis. Mutations were induced in wildtype male AB/TL fish by four rounds of 3 mM ENU treatment as previously described *(58)*.

An allelic series of predicted *lrp6* nonsense mutants (*u348, u349, u350* and *u351*) were recovered from founders mutated using CRISPR/Cas9. Briefly, *in vitro* transcribed, capped *cas9* mRNA and sgRNAs, prepared as described in *(59)* using T4 DNA polymerase (New England BioLabs, Ipswich, MA, USA) and mMessage mMACHINE (Ambion, Austin, TX, USA), complementary to exon 2 of *lrp6* (sg1: GGCCAACGCCACGCTGGTGA, sg2: GGCCAGACCGGAGATGACGG; Table S4) were microinjected into the cell of 1 cell stage embryos. Injected fish were raised to adulthood and genotyped for mosaicism of exon 2 using high resolution melting analysis (HRMA, see Table S5). Fish with a high degree of mosaicism were prioritized for outbreeding to generate F1s which were subsequently genotyped using headloop PCR combined with Sanger sequencing to identify alleles of interest *(60)* (Tables S3 and S5).

The *Tg(HSE:cachd1, EGFP)w160*, *Tg(neurod1:Cachd1-EGFP)w162* and *Tg(gng8:EGFP)u775* lines were generated by Tol2-mediated mutagenesis. Briefly, 1-cell zebrafish embryos were co-injected with *pTol2 HSE:cachd1, EGFP* (*w160Tg*), *pTol2 neurod1:cachd1-EGFP CG2* (*w162Tg*) or *pTol2 gng8:EGFP* (*u775Tg*) construct (25-50 pg; see below) and capped transposase mRNA (40 pg) and the embryos raised to adulthood. Offspring of the injected, adult fish were screened for germline transmission of the transgene and their progeny raised.

Cloning and genotyping of *u761*

Having used a combination of backgrounds to generate our F2s, we mapped *u761* in F3 embryos. We used bulked segregant analysis *(61)* followed by high resolution SSLP and SNP analyses to localize *u761* to a 0.28 MB interval on LG6 between a SNP in the first coding exon of *ak4* (2/5212 recombinants; *ak4* e1 primers; see Table S5) and an SSLP in intron 8-9 of *cachd1* (1/5212 recombinants; *cachd1* i8-9 primers; see Table S5). Sequencing of *cachd1* cDNA revealed a T to A transversion in the 24th exon of *cachd1* that causes a valine to aspartic acid amino acid substitution in its transmembrane domain (reverse strand 6:31607781 T>A, 1122V>D, Zv11 assembly). Mutants were subsequently genotyped with DCAPs primers (Table S5, *u761*-AloI primers) and the restriction enzyme AloI, which cuts the mutant allele, and then more routinely by KASP assay (see below).

Morpholino knockdown

Two non-overlapping morpholino antisense oligonucleotides for *cachd1* (MO1: GTGTATTTTCCTACCTGCATGGTGA; MO2: AGGGATGATGTCTAACTCACCTGCT) were obtained from GeneTools (Philomath, OR, USA) and microinjected into the yolks of 1-cell stage zebrafish embryos in 1 nL volumes for a total dose between 4 ng and 0.5 ng, depending upon the experiment.

DNA extraction, KASP and HRMA genotyping

Embryos or larvae were lysed at 95ºC in 25 mM KOH, 0.2 mM EDTA for 30 minutes, cooled to 4ºC and briefly vortexed to disrupt remaining tissue. The lysate was briefly spun in a centrifuge to collect, then neutralized with an equal volume of 40 mM Tris-HCl, pH 5.

KASP or HRMA genotyping of DNA lysates was performed as per manufacturer's instructions, using either 2× KASP Master Mix with standard ROX (LGC Biosearch Technologies, Hoddesdon, UK) or 2× Precision Melt Supermix (Bio-Rad, Hercules, CA, USA), respectively, and a Bio-Rad CFX96 qPCR machine (see Table S5 for primer details).

Melting curves from HRMA genotyping were analyzed using Precision Melt Analysis software (version 1.2; Bio-Rad).

cDNA and plasmid constructs

Total RNA was extracted and purified from pools of 10-20 embryos (wildtype, *rch*, or *cachd1* MO-injected, depending on experiment) with TRIzol reagent (Life Technologies, Grand Island, NY, USA) according to the manufacturer's instructions. cDNA was then produced using the SuperscriptIII first strand synthesis system for RT-PCR (Life Technologies; see Table S5).

pCS2+ cachd1-EGFP and *pCS2+ cachd1^{u761}-EGFP*: Full-length *cachd1* and *cachd1^{u761}* were amplified from cDNA with Phusion DNA polymerase (New England BioLabs) and primers tagged with SalI and SacII restriction enzymes sites (see Table S5 for primer sequences). The resulting PCR fragment and the *pEGFP-N1-1* vector were sequentially digested with SalI and SacII prior to ligation with Quick ligase (New England Biolabs) to make a *pcachd1-EGFP-N1-1* plasmid. The *pcachd1-EGFP-N1-1* construct was then cut with SalI and HpaI and the fragment containing *cachd1-EGFP* cloned between the SalI and SnaBI sites of the *pCS2+* vector.

pTol2 neurod1:cachd1-EGFP CG2: Full-length *cachd1-EGFP* was PCR-amplified from *pCS2+ cachd1-EGFP* plasmid with AttB1-tagged primers. The Gateway cloning method was

used to combine this PCR product with *pDONR 221*, *p5E NeuroD*, *p3E polyA* and *pDest tol2 CG2* following the manufacturer's protocols.

pTol2 HSE:cachd1, EGFP: Full-length *cachd1* was amplified from cDNA using high-fidelity Phusion DNA polymerase (New England Biolabs) and then phosphorylated with PNK (New England BioLabs; see Table S5 for primers). The phosphorylated fragments were then cloned into the StuI site of a *pCS2+* vector treated with Antarctic Phosphatase (New England Biolabs) to prevent recircularization. The resulting vectors were cut with BamHI and SnaBI and the *cachd1*-containing fragments cloned into the BamHI and EcoRV sites of the *pTol2 HSE:EGFP* vector *(62)* to obtain the *pTol2 HSE:cachd1, EGFP* construct for injection.

pTol2 gng8:EGFP: a 3060 bp promoter region of the *gng8* gene was amplified by PCR (see Table S5 for primer details) and cloned into a *TOPO-TA* vector. This fragment was subcloned into *pEGFP-N1,* upstream of the *EGFP* open reading frame, and the subsequent *gng8:EGFP* fragment cloned into *pTol2*.

For flow cytometry protein production, the coding sequence for the ectodomain of human and zebrafish *CACHD1* (truncated before the transmembrane domain at P1095/P1108 respectively) was codon optimized for HEK cells and synthesized by GeneArt (Thermo Fisher Scientific, Waltham, MA, USA). These fragments had NotI and AscI target sequences at the 5′ and 3′ ends, respectively, for subcloning into prey protein and ectodomain bait protein production vectors.

Human and zebrafish CACHD1 prey protein expression constructs (ectodomain fused to a COMP domain, β-lactamase domain and FLAG tag) and zebrafish Cachd1 ectodomain production constructs (ectodomain fused to hexahistidine and BirA ligase peptide substrate tags) were prepared by NotI/AscI restriction enzyme double digest (New England Biolabs) of *pTT3*-based vector backbones *(63)* (Addgene IDs 71471 and 36153) and shuttle vectors containing the synthesized fragments, followed by ligation with T4 ligase (New England Biolabs). The resulting constructs were screened by Sanger sequencing to confirm correct in-frame insertion.

To create human and zebrafish FZD-EGFP bait protein constructs, IMAGE consortium clones *(64)* (see Table S6 for details) were used as templates in PCR reactions to generate full length inserts (including the seven transmembrane domains) with NotI and AscI target sequences at the 5′ and 3′ ends, respectively, except for *fzd4* and *fzd9a* where the insert was synthesized by GenScript (Piscataway, NJ, USA) as no complete full length clone was available. *fzd1* and *fzd8b* both had NotI/AscI restriction sites in the respective coding sequences, so fusion PCR was used to generate full length inserts with synonymous mutations in the recognition sequences (see Table S5 for primer sequences). The PCR products were purified using a Qiaquick PCR purification kit (Qiagen, Hilden, Germany) and then digested with NotI/AscI (New England Biolabs) and ligated to a *pTT3* vector containing *EGFP* (see below). The resulting constructs were verified by Sanger sequencing.

The *pTT3-EGFP* vector was constructed by replacing the C-terminal tag encoding region of a bait protein vector *(65)* (Addgene ID 36150) with *EGFP*. The bait protein vector was digested with AscI/BamHI (New England Biolabs) to remove the tag encoding region and then ligated to an *EGFP* insert generated by PCR using primers with AscI and BamHI tails (see Table S5 for primer sequences). The resulting vector was verified by Sanger sequencing to ensure in-frame insertion of the EGFP coding sequence.

All constructs used for producing proteins for surface plasmon resonance and crystallography were based on the mammalian stable expression vector *pNeoSec (66)*. Mouse CACHD1 extracellular domain (UniProt: Q6PDJ1, residues D50–S1107) was derived from IMAGE clone 6834428 (Table S6; Source Bioscience). Mouse FZD5 cysteine rich domain (UniProt: Q9EQD0, residues A27-T157), human FZD7 CRD (UniProt: O75084, residues Q33-G170), human FZD8 CRD (UniProt: Q9H461, residues A28-T158) were synthesized (GenScript). Human $LRP6_{P1E1P2E2}$ (UniProt: O75581, residues A20-P630) and $LRP6_{P3E3P4E4}$ (residues V629-G1244) domains were described previously *(51)*.

Tissue culture and cell transfection

HEK293T (ATCC: CRL-3216), APC4 (APC4 line was generated from HEK293T cells by CRISPR targeting *APC* with truncation at 1225 a. a.) *(48)*, SW480 (ATC: CCL-228), Ls174T (ATC: CL-188), DLD1 (ATC: CCL-221) and HCT116 (ATC: CCL-247) were maintained in DMEM GlutaMAX (GIBCO) supplemented with 5% fetal bovine serum (FBS) (GIBCO), 100 U/mL penicillin (GIBCO) and 100 mg/mL streptomycin (GIBCO). All cells were maintained at 37°C in an incubator with 5% CO_2. Cells were seeded in plates 24 hours before transfection, and plasmids were transfected using polyethylenimine (PEI; Polysciences, Warrington, PA, USA) or Fugene 6 (Promega) according to the manufacturer's instructions.

HEK293T cells were simultaneously transfected with 1 µg *pCS2Cachd1-EGFP* or *pCS2Cachd1_V1122D-EGFP* and 1 µg *KDEL-tRFP* plasmid using Fugene 6 transfection reagent (Promega). EGFP/tRFP expression was confirmed 24 hours post transfection and the cells fixed at 42 hours post transfection and imaged on a spinning disk microscope (see below).

For protein production and flow cytometry experiments, suspension cultures of HEK293E *(67)* or HEK293-6E *(68)* cells were transfected using linear PEI:plasmid complexes, incubated for between 2-6 days and then harvested by centrifugation. The resulting cells or conditioned media were then used for downstream experiments *(63)*. Briefly, HEK293E or HEK293-6E cells were maintained in suspension cultures in Freestyle 293 Expression Media (Gibco, Waltham, MA, USA) supplemented with heat-inactivated fetal calf serum (1%) and G418 (geneticin, 50 µg/mL; Sigma-Aldrich, St. Louis, MO, USA), routinely maintained at densities between 2.5×10^5 and 4×10^6 cells/mL in Erlenmeyer flasks (Corning, Corning, NY, USA) in a humidified orbital shaker at 37ºC, 5% CO_2. One day before transfection, cultures were split down to 2.5×10^5 cells/mL in standard media or, in the case of biotinylated protein production, media supplemented with D-Biotin (100 µM). Plasmids for transfection were prepared using PureLink HiPure Plasmid Maxiprep kit, as per manufacturer's instructions (Thermo Fisher Scientific), and resuspended in ddH_2O at 1 mg/mL. For each transfection, purified plasmid was mixed with linear 25 kDa PEI (Polysciences) at a ratio of 1 µg DNA:2.2 µg PEI (per 5×10^6 cells) in unsupplemented Freestyle 293 Expression Media (1/10th culture volume), vortexed and left to stand for 5 minutes at room temperature to allow complexes to form, before mixing into the cell cultures (for example, to transfect a 50 mL culture with density 5×10^5 cells/mL, 50 µL of plasmid was mixed with 110 µL PEI 1 mg/mL in water, in 2 mL media). In the case of biotinylated protein production, cells were co-transfected with an additional secreted BirA ligase plasmid *(63)* (Addgene ID 64395) included in the transfection mixture at a ratio of 10 µg DNA:22 µg PEI: 1 µg BirA. Transfected cultures were incubated for approximately 2 (for flow cytometry) or 6 days (protein production) before harvesting by centrifugation (200 × g or 3200 × g, respectively) to separate cells from conditioned media.

Proteins used in surface plasmon resonance and crystallography were derived from stable cell lines established by G418 selection (1 mg/mL, Sigma) of transfected HEK293S GnTI(−) cells *(69)*.

Organoid culture

Organoids were cultured as described in *(70)*, except that Matrigel was replaced with Cultrex© BME, Type 2 RGF PathClear (Amsbio, Abbingdon, UK, 3533-010-02). Briefly, organoid basal media contains EGF (Invitrogen, Waltham, MA, USA PMG8043), NOGGIN and RSPONDIN1 (ENR). NOGGIN and RSPONDIN1 conditioned media (CM) were generated from HEK293T cells. APC5 organoids were previously generated by CRISPR/Cas9, generating a truncation in APC at 680 aa *(48)*. WNT3A CM was generated from L cells (ATCC: CRL-2647).

TOPFlash assay

HEK293 SuperTopFlash cells (STF, ATCC: CRL-3249) were seeded into a 96-well plate (10^5 cells/well) and transfected with a constitutive Renilla luciferase plasmid (pRL-tk; Promega) together with an expression plasmid of mouse *Cachd1* (ectodomain only, transmembrane with cytoplasmic domain or full length) or a control plasmid (expressing bacterial T7 polymerase) with lipofectamine 2000 (Invitrogen). All plasmids were transfected at a concentration of 10 ng/mL. Twenty-four hours after transfection, the media was replaced either by conditional media from normal L cells (control, ATCC: CRL-2648) or from a WNT3A producing L cell line (ATCC: CRL-2647). Firefly and Renilla luciferase activities were measured 24 h later using the Dual-Glo luciferase reporter assay system (Promega) with an Ascent Lunimoskan luminometer (Labsystems). Firefly luciferase activity was normalized to the constitutive Renilla luciferase activity.

Protein production and purification

Conditioned media was harvested from transfected cultures, pooled and filtered through 0.2 μm filters and stored at 4˚C until use.

Prey protein transfections were quantified by β-lactamase assay, measuring the turnover of nitrocefin substrate by changing absorbance at 485 nm over time *(63)*, then normalized by dilution.

Biotinylated bait ectodomain transfections were dialyzed against PBS using SnakeSkin dialysis tubing (molecular weight cut-off 10,000 Da; Thermo Scientific) and several buffer changes (approximately 25 – 30 L in total). Biotinylated protein concentration was quantified by ELISA, using streptavidin-coated microplates and a monoclonal antibody to detect the CD4d3+4 tag *(63)* (Nunc Immobilizer, Thermo Fisher Scientific).

Unbiotinylated ectodomain transfections were collected and quantified by ELISA using nickel-coated microplates and pooled for purification using nickel-sepharose columns (HisTrap HP, GE Healthcare, Chicago, IL, USA) and an AKTAxpress chromatography system (GE Healthcare). Briefly, nickel-charged columns were pre-eluted with elution buffer (10 mM Na_2HPO_4, 10 mM NaH_2PO_4, 0.5 M NaCl, 0.4 M imidazole, pH 7.4, filtered and degassed under vacuum) then equilibrated with running buffer (10 mM Na_2HPO_4, 10 mM NaH_2PO_4, 0.5 M NaCl, 0.04 M imidazole, pH 7.4, filtered and degassed under vacuum). Pooled supernatants were adjusted to approximately 0.1 M NaCl and 0.01 M imidazole then run through the column at a flow rate of 1 mL/min. The column was washed with 15 volumes of running buffer and then eluted in 0.5 mL fractions with 10 columns of elution buffer. Peak

fractions were pooled and dialyzed against PBS, then quantified by absorption at 280 nm using a Nanodrop 1000 instrument (Thermo Fisher Scientific).

Proteins used in surface plasmon resonance and crystallography were purified from conditioned medium collected from stable cell line cultures. The media was buffer exchanged with PBS and His-tagged proteins were captured with 5 mL HisTrap Excel columns (GE Healthcare), washed with 20 mM imidazole and eluted with 300 mM imidazole containing PBS buffer. The eluted proteins were further purified using a Superdex 200 16/60 column (GE Healthcare), in a buffer of 10 mM HEPES, pH 7.4, 150 mM NaCl. Before crystallization, purified glycoproteins were deglycosylated using EndoF1.

Antibody generation and purification

To characterize the expression pattern of the receptor protein, we raised and affinity purified a polyclonal antibody against the recombinant extracellular domain of zebrafish Cachd1.

Briefly, purified zebrafish Cachd1 ectodomain was prepared (see above) and sent to Cambridge Research Biochemicals (Billingham, United Kingdom) for a rabbit immunization protocol. Activity against the Cachd1 ectodomain in rabbit blood sera was confirmed by ELISA. The blood serum was then affinity purified against biotinylated recombinant ectodomain immobilized on a streptavidin sepharose column, using an AKTAxpress chromatography system. Purified antibodies were eluted in fractions using a low pH buffer, then immediately neutralized. Peak fractions were tested for anti-Cachd1 activity, then pooled and dialyzed against PBS. Total protein concentration was determined by absorbance at 280 nm by Nanodrop. The affinity purified antibody was checked for purity by SDS-PAGE and then validated by western blot, immunohistochemistry and flow cytometry (see Fig. S1) *(38)*.

Retrogenix Cell Microarray Technology

Cell Microarray Technology *(71)* was used to identify potential binding partners for multimerized human CACHD1 ectodomain (prepared as above) and was performed by Charles River Discovery Research Services UK Limited (formerly Retrogenix Limited; Chinley, United Kingdom; for bait target details, see *(72)*).

Flow cytometry

To test Cachd1 prey binding interactions, live suspension culture HEK293E cells transfected with *FZD-EGFP* constructs (and mock transfected control cells) were split into samples of 2.5-5.0 × 10^5 cells in 1% BSA in PBS and placed in individual wells of 96 well round bottomed culture plates on ice. The cells were collected by centrifugation (200 × g for 5 minutes at 4°C) and then resuspended in dilutions of prey protein (human or zebrafish Cachd1 and mouse CD200R; batchwise dilution determined by β-lactamase assay, see above) or 1% BSA in PBS (secondary only controls), and incubated on ice for 30 minutes. The cells were washed three times, by centrifugation and resuspension in PBS, then incubated in anti-FLAG-phycoerythrin secondary antibody diluted in 1% BSA in PBS (Antibody registry ID: AB_1268475, mouse IgG1, 1:500, Abcam) for a further 30 minutes. Cells were washed three times, by centrifugation and resuspension in PBS, then analyzed using a LSRFortessa flow cytometer with a 5-decade logarithmic scale for detection, a high throughput sampler for 96 well plates and FACSDiva software (BD Biosciences).

Where possible, we verified the surface expression of bait proteins or EGFP-tagged Cachd1 in live cultures by following the same protocol but using specific primary antibodies in place

of prey proteins (Fig. S1A, S14E; anti-Cachd1, diluted 1:700, bespoke rabbit polyclonal, see above; OMP-18R5, human anti-FZD7 IgG *(33)*, diluted 1:2000, OncoMed Pharmaceuticals; anti-Smo, AB_1270802, rabbit polyclonal, diluted 1:500, Abcam; anti-Jamb, bespoke goat polyclonal, diluted 1:200, Everest Biotech) and Alexa Fluor-conjugated secondary antibodies (Molecular Probes, diluted 1:500).

The same procedure was followed for experiments testing the ability of OMP-18R5 to block Cachd1 prey-FZD-EGFP interactions, but with an additional incubation step before the application of prey proteins: cells were resuspended in OMP-18R5 diluted in 1% BSA in PBS (1:800) or 1% BSA in PBS only (control) and incubated for 30 minutes on ice, washed three times in PBS, and then resuspended in prey protein dilutions.

Mock transfection controls were used to determine forward and side scatter voltages for samples prior to data collection, and for background gating thresholds in data analysis. "Cells only" (no prey/primary or secondary antibodies) and "secondary antibody only" controls were included in every experiment. Flow cytometry data was analyzed using FlowJo V10 (FlowJo, Ashland, OR, USA). Single cell populations were isolated using forward and side scatter values, bisected into EGFP-negative (untransfected) and EGFP-positive subpopulations and then the median value for phycoerythrin fluorescence (indicating prey binding) calculated for each (Fig. S14B). Binding of prey protein to EGFP-positive cells was quantified by taking the ratio of the medians: $\Delta M_{PE} = \ln\left(M_{PE}^{EGFP+}/M_{PE}^{EGFP-}\right)$.

Surface Plasmon Resonance

Biotinylated proteins (FZD5/7/8$_{CRD}$ and LRP6$_{P1E1P2E2}$ or LRP6$_{P3E3P4E4}$) were obtained by co-transfection of avi3-tagged constructs *(73)* and a BirA-ER plasmid into HEK293T cells. About 500-1,000 resonance units of each of the biotinylated proteins were immobilized on a SA sensor chip (GE Healthcare), using a Biacore S200 machine (GE Healthcare) at 25 °C with a running buffer comprising 10 mM HEPES, pH 7.5, 150 mM NaCl and 0.005% Tween 20. A dilution series of purified CACHD1$_{ECD}$ analyte was passed over the flow cells at high flow rate (100 µL/min) and the real-time response recorded at a frequency of 10 Hz. The response was plotted versus the concentration of the analyte and fitted by nonlinear regression to a one-site saturation binding model (Sigma Plot, Systat software, Inc. San Jose, CA).

Crystallization, data collection and structure determination

CACHD1$_{ECD}$ was concentrated to 5 mg/mL and mixed with equal molar of FZD5$_{CRD}$ and LRP6$_{P3E3P4E4}$. Crystallization screening was carried out using the sitting-drop vapor diffusion method in 96-well plates. The crystals were obtained in conditions of 0.1 M Calcium acetate; 0.1 M Sodium acetate, pH 4.5; 10% (w/v) PEG 4000.

Crystals were flash frozen by immersion in a reservoir solution supplemented with 25% (v/v) glycerol followed by transfer to liquid nitrogen, and kept at −173 °C during X-ray data collection at I03, Diamond Light Source, with a wavelength of 0.9762 Å. The best diffracted crystal shows resolution of 4.7 Å, with space groups of $C2_1$. Structure determination by molecular replacement with components structures solved in our laboratory and refinement used PHENIX *(74)* to good R factors and bond angles (see Table S2 for data collection and refinement statistics). The ternary complex structure was deposited at the Research Collaboratory for Structural Bioinformatics Protein Data Bank under accession number 8S7C.

In situ hybridization and Immunohistochemistry

Embryos or larvae were fixed in 4% paraformaldehyde and *in situs* performed following standard protocols *(75)*. To create plasmid templates for *in situ* probe generation, regions of the *zgc:101731, slc18a3b, aoc1* and *cachd1* genes were PCR-amplified (see Table S5 for primer sequences) and TA-cloned into the *pCRII* vector. The *kiss1 in situ* probe template was generated directly by PCR (see Table S5). Previously published *in situ* probes used include (see Table S7 for references): *kctd12.1, kctd12.2, kctd8, axin2, lft1, otx5, spaw, selenop2, prss1, aldh1a3, dbx1b, wnt3a, lef1*. All enzymes used for plasmid linearization and *in vitro* transcription are listed in Table S7. Antisense probes were generated with digoxigenin and fluorescein labelling kits (Roche). Anti-digoxigenin-AP and anti-fluorescein-AP antibodies (Antibody registry ID: AB_2734716 and AB_2734723 respectively, Roche) coupled with 5-bromo-4-chloro-3′-indolyphosphate and nitro-blue tetrazolium chloride were used to visualize colorimetric *in situs*. Anti-digoxigenin-POD and anti-fluorescein-POD antibodies (AB_514500 and AB_840257 respectively, Roche) and Alexa Fluor-conjugated tyramides (Molecular Probes) were utilized for detection in fluorescent *in situ* hybridization.

In situ hybridization chain reaction was performed according to published protocol *(76)* using Alexa Fluor-conjugated hairpin amplifiers and hybridization buffers from Molecular Instruments Inc. (Los Angeles, CA, USA). Probe sets for *cachd1* and *lrp6* are detailed in Table S8.

For immunohistochemistry, embryos were stained according to published protocol, except for using freshly fixed embryos without storage in methanol *(77)*. Antibodies used in this study were: anti-acetylated α-tubulin (Antibody registry ID: AB_477585, clone 6-11B-1, mouse IgG2b, Sigma, diluted 1:250 in blocking solution), anti-SV2 (AB_2315387, mouse IgG1, deposited to the Developmental Studies Hybridoma Bank by Buckley, K.M., diluted 1:250), anti-HuC/HuD (AB_221448, clone 16A11, mouse IgG2b, Molecular Probes, diluted 1:250), anti-phospho-S10-histone H3 (AB_443110, mouse IgG1, Abcam, diluted 1:250), anti-Cachd1 (this study, rabbit polyclonal, diluted 1:50), anti-GFP (AB_10013661, rabbit polyclonal, Torrey Pines Biolab, diluted 1:1000; or AB_300798, chicken polyclonal, Abcam, diluted 1:500). The use of anti-PCNA (AB_2160343, clone PC10, mouse IgG2a, Cell Signaling Technology, diluted 1:100) required heat-mediated antigen retrieval: embryos were incubated in 10 mM Sodium citrate in PBS, pH 6.0, at 85°C for 20 mins before blocking. Alexa Fluor-conjugated anti-mouse IgG subtypes/rabbit/chicken secondary antibodies (Molecular Probes) were diluted 1:200 in blocking solution before use. 4′,6-diamidino-2-phenylindole (DAPI, Invitrogen) was added to embryos (10 µg/mL in PBST) to counterstain nuclei before imaging.

Quantitative RT-PCR

RNA was extracted from cell culture or organoids according to the manufacturer's instructions (Qiagen RNeasy; Qiagen). cDNA was prepared using Maxima first strand cDNA synthesis kit with dsDNase (#1672, Thermo Fisher Scientific). Quantitative PCR detection was performed using PowerUp SYBR Green Master Mix (A25742, Applied Biosystems, Waltham, MA, USA). Assays for each sample were done in triplicate and were normalized to housekeeping genes *ACTB* (human *β-ACTIN*) or *Hrpt1* (mouse). Primer sequences are listed in Table S5.

Heat shock, laser cell ablation, BrdU, labelling of habenular projections and transplantation experiments

For rescue experiments, embryos transgenic for *Tg(HSE:cachd1, EGFP)w160* were heat shocked for 30 minutes in a 40˚C water bath, then raised at standard temperature to 4 dpf and fixed in 4% paraformaldehyde.

Laser cell ablation, BrdU incorporation experiments and lipophilic dye (DiI/DiD) labelling of habenular efferent projections were performed as previously described *(19)*.

Transplantation experiments were also done as previously described *(19)* using embryos from *Et(gata2a:EGFP)pku588*, *cachd1*$^{u761/+}$ incrosses as donors and fixing host embryos at 56 hpf or 4 dpf.

Imaging

For transmitted light pictures, larvae were mounted in glycerol and imaged using differential interference contrast optics (Leica CTR6000; 20× and 40× objectives; Leica Microsystems, Wetzlar, Germany). For confocal microscopy, heads were mounted in 1.2% low-melt agarose in glass-bottom dishes (MatTek, Ashland, MA, USA or LabTek, Grand Rapids, MI USA). Fluorescence was imaged by confocal laser scanning microscopy (Leica TCS SP5 and Leica TCS SP8) using a 40× oil-immersion objective (40× 1.3 Oil DIC III) or a 25× water-immersion objective (25× 0.95), and z stacks were acquired in 0.75 – 2 μm intervals. Cell cultures were imaged using a Marianis Spinning Disk (Intelligent Imaging Innovations, Inc., Denver, CO USA) system. 3D reconstructions and maximum-intensity projections were generated from stacks of images with Volocity (Improvision, Coventry, UK) and ImageJ (NIH). Image segmentation and quantification was performed using IMARIS (v8.0.1, Bitplane, Zurich, Switzerland).

Statistics

Statistical analysis was performed using RStudio (v1.4.1106, base R x64 v4.0.5, DescTools package v0.99.44) and Microsoft Excel 2010. Charts were plotted using the ggplot2 package (v3.3.3).

Descriptive statistics, scatterplots and normalized histograms for flow cytometry experiments were generated in FlowJo V10 (FlowJo, Ashland, OR, USA).

The Q′ test for equal proportions and modified Marascuilo procedure for multiple testing (using a Wilson variance calculation) are described in *(78)*. Where the proportion was $0.1 < \hat{p} < 0.9$ and/or $n > 20$, confidence intervals were calculated using a normal assumption; otherwise by the Wilson count method. Fisher's exact tests were used in place of χ^2 where expected values were below 5.

Manuscript and figure preparation

The manuscript was prepared according to the ARRIVE guidelines for reporting animal research *(79)*.

Figures were compiled using Adobe Photoshop CS6 (64 bit).

Fluorescent and confocal microscopy images were adjusted globally for brightness and contrast using FIJI (v1.53n), scale bars added and then flattened into RGB images and exported as TIFFs.

Color balance of wholemount *in situ* hybridization images was adjusted in Adobe Photoshop CS6 (64 bit).

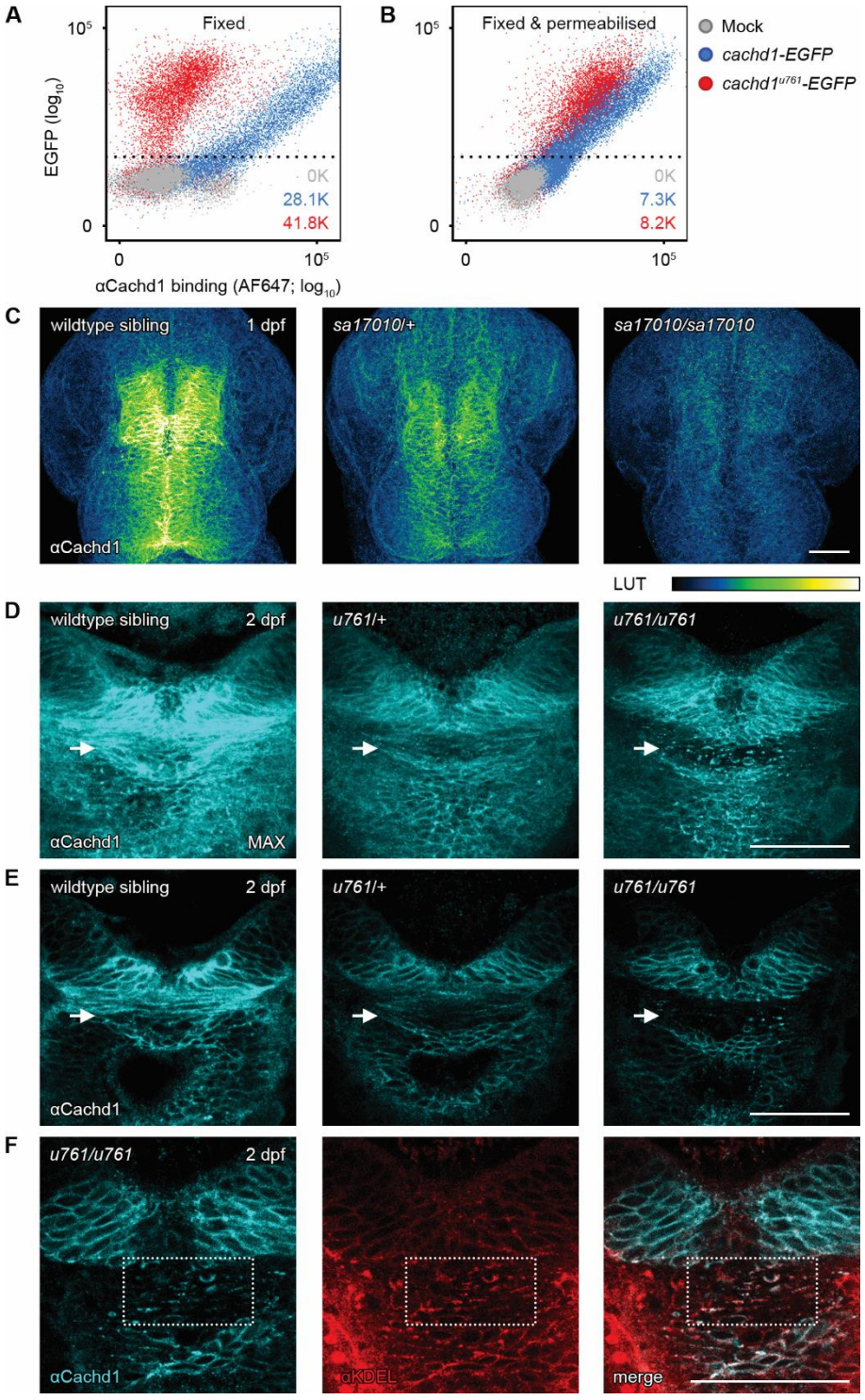

Fig. S1. Cross-validation of *cachd1* mutations and anti-Cachd1 antibody.
(**A** and **B**) Flow cytometry of untransfected (Mock, grey) and transfected HEK293E cells expressing wildtype Cachd1- (blue) or mutant Cachd1^{u761}-EGFP (red) fusion proteins stained with anti-Cachd1 antibody after fixation (A) and permeabilization (B). The mutant fusion protein was stained strongly after permeabilization of the cells, suggesting the protein was not trafficked to the plasma membrane. Numbers in each panel indicate the total number of EGFP-positive events recorded. (**C**) Dorsal views of brains of 1 dpf siblings from a *cachd1*$^{sa17010/+}$ incross,

stained with anti-Cachd1 antibody. Note that the *sa17010* allele has an early nonsense mutation that is expected to prevent translation of the protein. Intensity of staining of the midbrain roofplate and dorsal diencephalon is correlated to *sa17010* genotype (see Table S1), indicating the antibody is specific for Cachd1. Maximum projections of confocal stacks. (**D**, **E** and **F**) Dorsal views of 2 dpf *cachd1*$^{u761/+}$ incross embryos stained with anti-Cachd1 antibody (D, E and F; cyan) and anti-KDEL (F; red). Note the punctate expression in the posterior commissure (white arrows in D, D′) in *u761* homozygotes, and the colocalization with ER resident proteins, marked by the anti-KDEL antibody (dotted box in F), indicating retention of the mutant protein. Representative maximum projection (D), single plane images from the same confocal stacks (E) or single plane confocal images (F). Scale bars = 50 µm.

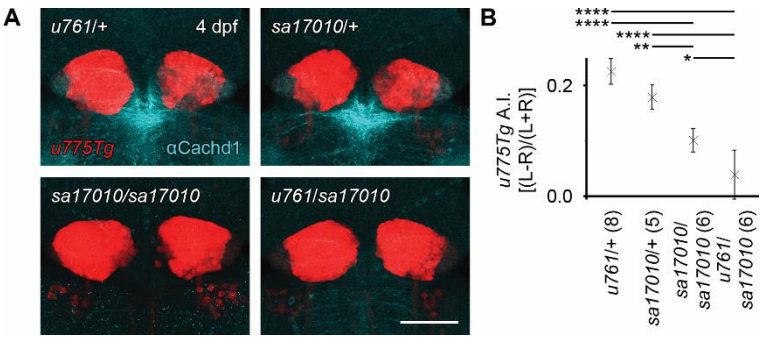

Fig. S2. The *sa17010* allele of *cachd1* phenocopies, and is unable to complement, *u761*. (**A**) Dorsal views of 4 dpf *Tg(gng8:EGFP)u775/o* larvae carrying *u761* and/or *sa17010* alleles of *cachd1*, stained with anti-Cachd1 antibody (cyan). *Tg(gng8:EGFP)u775* expresses EGFP in differentiated dorsal habenula neurons (red). Right habenula labelling is larger in the *sa17010* and *u761/sa17010* larvae than in heterozygotes, indicating bilateral 'double left' symmetry. Maximum projections of confocal stacks. Scale bar = 50 µm. (**B**) Asymmetry index calculated from EGFP habenulae volumes of *u761/+*, *sa17010/+*, *sa17010/sa17010* and *u761/sa17010* 4 dpf larvae. *sa17010* homozygotes and *u761/sa17010* transheterozygotes are bilaterally symmetric, suggesting loss of function of *cachd1* is causative of the *rorschach* phenotype. Number of larvae analyzed indicated in brackets. Error bars represent 95% confidence intervals of the mean. ANOVA (degrees of freedom = 3, $F = 27.41$, $P = 1.9 \times 10^{-7}$) and *post hoc* Tukey pairwise comparisons was used for hypothesis testing, * $0.1 \geq P > 0.05$, ** $0.05 \geq P > 0.01$, **** $P \leq 0.005$.

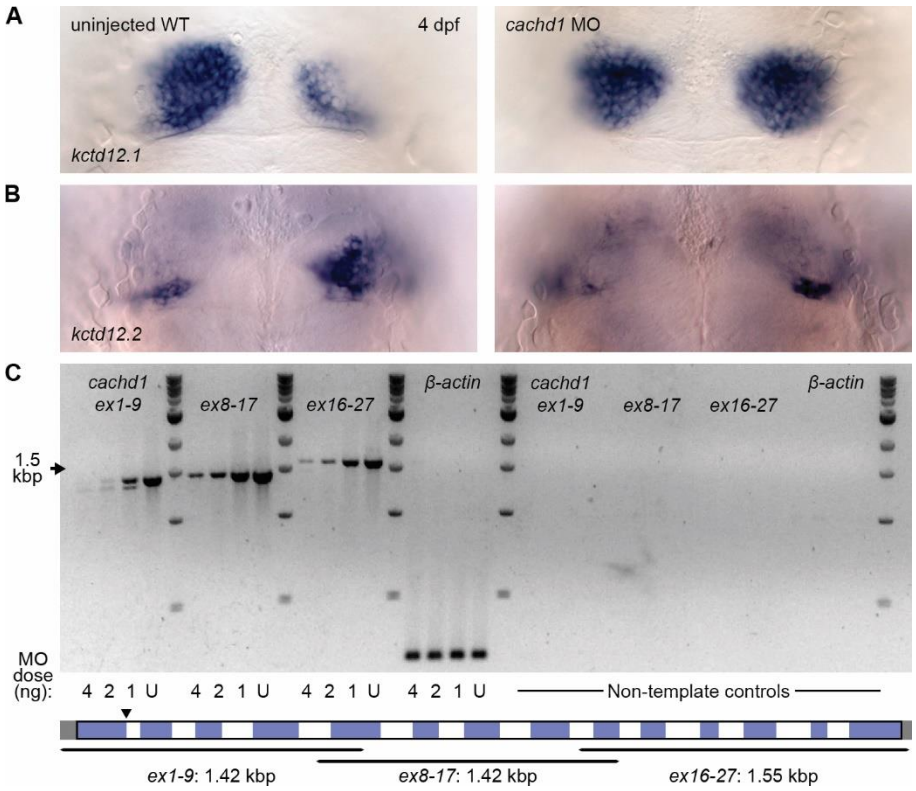

Fig. S3. Morpholino knockdown of *cachd1* results in bilateral symmetry.
(**A**-**B**) Dorsal views of 4 dpf uninjected wildtype and *cachd1* morpholino-injected larvae after wholemount *in situ* hybridization using antisense riboprobes against asymmetric dorsal habenula markers *kctd12.1* (A, n = 253/263) or *kctd12.2* (B, n = 16/17). Note the increase in *kctd12.1* expression and corresponding decrease of *kctd12.2* expression in the right habenula of *cachd1* morphants. (**C**) Semi-quantitative RT-PCR for *cachd1* transcripts (three primer sets spanning exons 1-9, exons 8-17 and exons 16-27) and reference gene *β–actin* in uninjected embryos (U) and those injected with ~4 ng, 2 ng and 1 ng of *cachd1* morpholino (MO1) showing a dose dependent reduction in *cachd1* expression and mis-splicing (exon 1-9). Subsequent Sanger sequencing of the RT-PCR products indicated mis-splicing resulted in an 89 bp deletion from the 3' end of exon 1 and usage of a cryptic donor site. Bottom panel: Schematic of *cachd1* transcript structure (ENSDART00000087964 Zv11, approximately to scale; alternating exons in blue/white and grey unannotated UTRs) with expected sizes of RT-PCR products indicated. The splice junction targeted by MO1 is indicated with a black arrowhead.

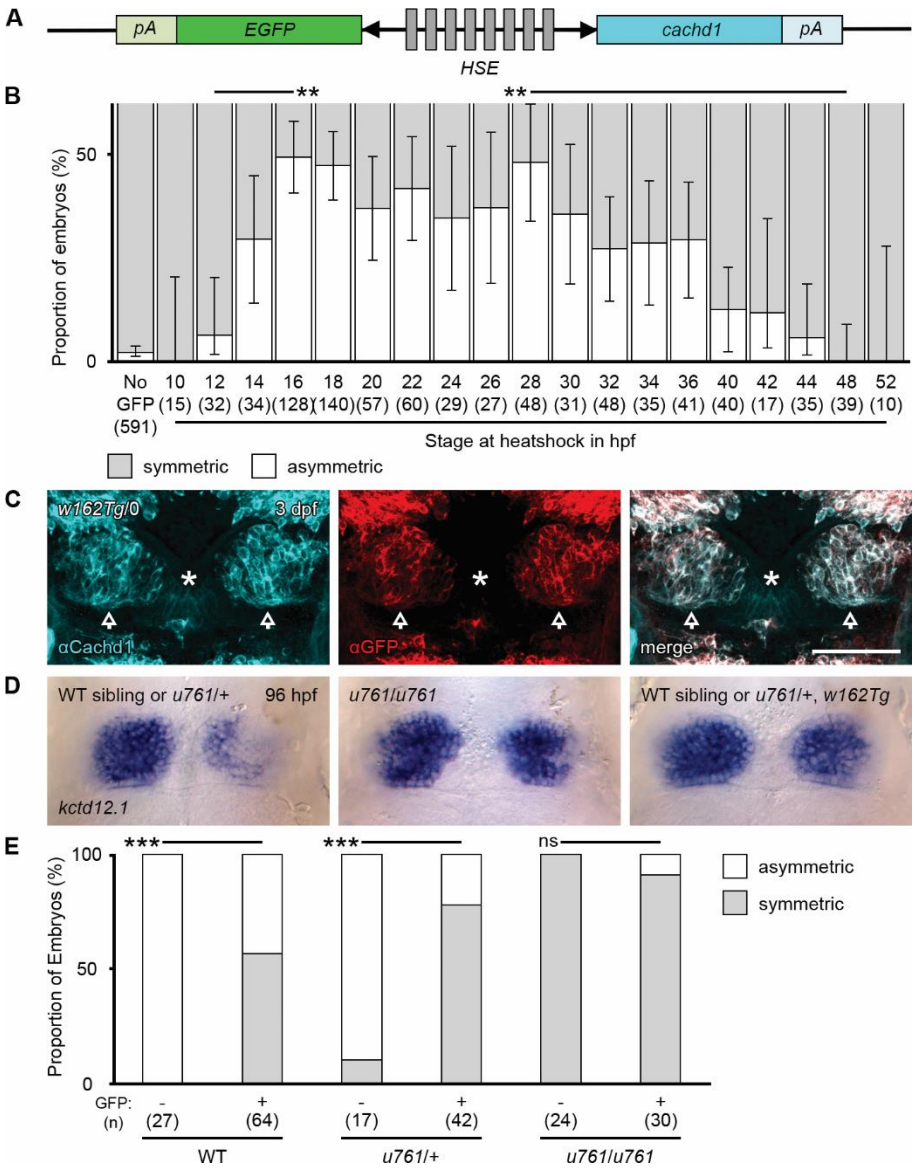

Fig. S4. Asymmetry in *cachd1*^{u761} mutants is restored by global overexpression of wildtype *cachd1*, but not in post-mitotic neurons.

(**A**) Schematic of construct used to generate transgenic *Tg(HSE:cachd1, EGFP)w160* fish. A bidirectional heat shock promoter (HSE) drives simultaneous expression of EGFP and Cachd1 in response to acute exposure to heat. (**B**) Chart showing the percentage of GFP-positive, *cachd1*^{u761} mutant larvae with symmetric (grey) or asymmetric (white) *kctd12.1* expression at 4 dpf, after receiving a heat shock at the stage indicated (GFP-negative, heat-shocked sibling larvae included in 'No GFP' column). There was substantial restoration of asymmetry after heat shock between 16 - 28 hpf, after which the proportion of larvae with wildtype phenotype declined. Number of larvae indicated in brackets. Error bars represent 95% confidence interval for the proportion, calculated using a normal approximation, or Wilson score when the proportion was less than 0.1, and/or the number of larvae tested was less than 20. Q′ test of equality of proportions (degrees of freedom = 19, $\chi^2 = 342.27$, $P = 4.0 \times 10^{-61}$) and *post hoc* modified Marascuilo procedure for multiple comparisons of proportions with Benjamini-Hochberg correction for multiple testing was used to test significance, ** $0.05 \geq P > 0.01$. A

limited number of statistically significant differences are presented here for clarity. (**C**) Dorsal views of *Tg(neurod1:cachd1-EGFP)w162* 3 dpf larvae stained with antibodies against Cachd1 and GFP. Ectopic expression of EGFP-tagged Cachd1 protein in post-mitotic neurons is driven by a *neurod1* promoter. Note the endogenous Cachd1 protein expression in the periventricular zone (asterisk) that does not co-localize with GFP antibody labelling in the dorsal habenulae (arrowheads). Representative maximum projections of confocal stacks. Scale bar = 50 μm. (**D**) Representative images of *in situ* hybridization with *kctd12.1* riboprobe in 96 hpf wildtype or *u761* heterozygous siblings (left panel), *u761* mutants (middle panel) or *w162Tg* transgenic, wildtype or *u761* heterozygotes (right panel). Note that overexpression of exogenous Cachd1-EGFP did not rescue the *u761* symmetry phenotype, and also resulted in bilateral symmetry in wildtype and heterozygous siblings. (**E**) Quantification of *kctd12.1 in situ* asymmetry phenotype in embryos expressing (+) or not expressing (-) the *neurod1:cachd1-EGFP* transgene. Number of embryos for each condition is brackets below each bar. Fisher's exact test, *** $0.01 \geq P > 0.005$.

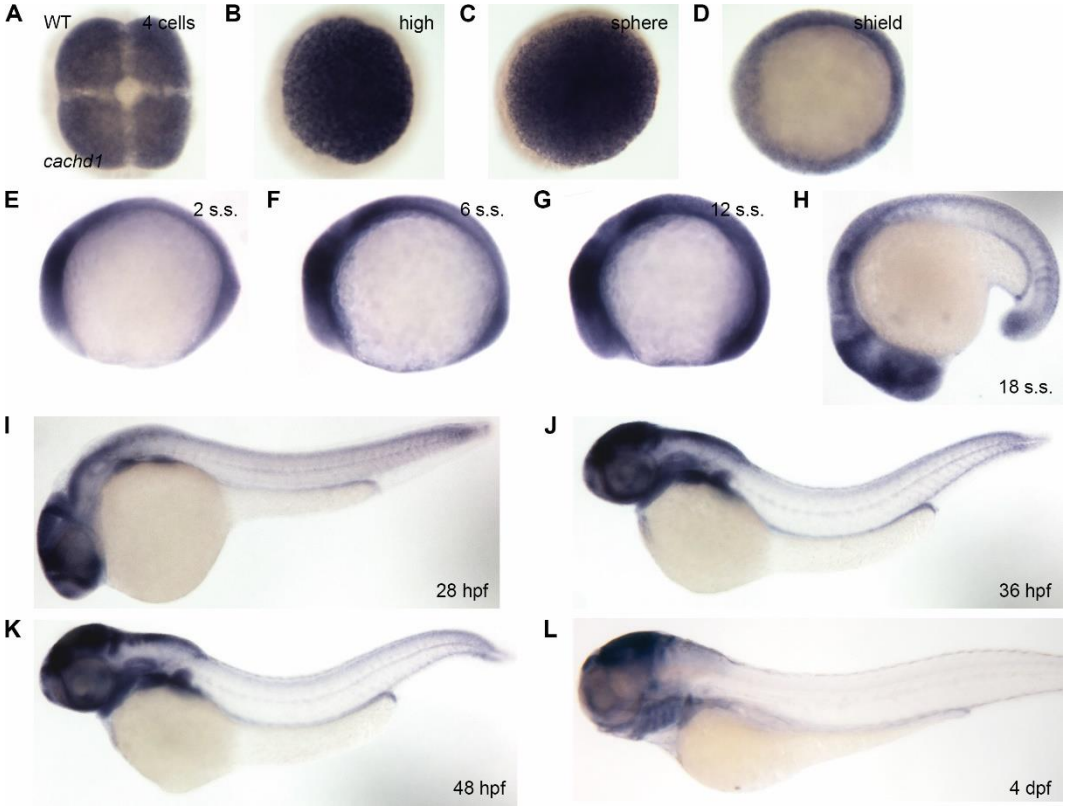

Fig. S5. Spatiotemporal pattern of *cachd1* gene expression.
(**A-L**) Representative images of colorimetric *in situ* hybridization with *cachd1* antisense riboprobe using whole wildtype embryos at different stages (indicated in each panel). Abbreviation s.s.: somite stage.

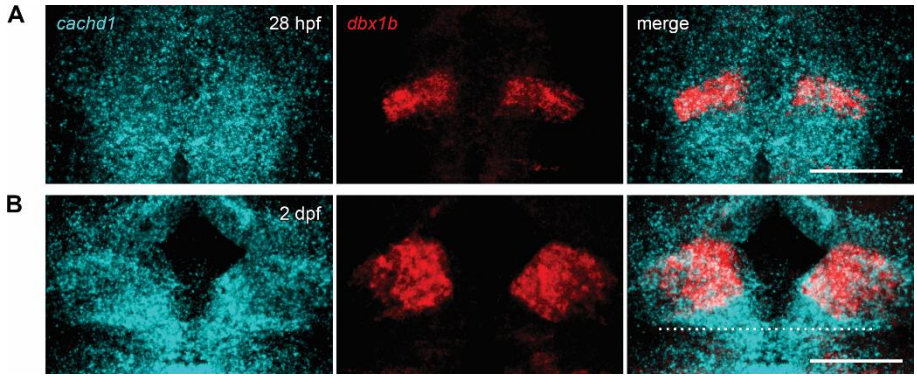

Fig. S6. *cachd1* is expressed by presumptive habenula neuron progenitors.
(**A**, **B**) Dorsal views of habenulae after double fluorescent *in situ* hybridization with *cachd1* antisense riboprobe (cyan) and the habenula neuron progenitor marker *dbx1b* (red) at 28 hpf (A) and 2 dpf (B). A single dotted line in (B) indicates the approximate position of the posterior commissure. Maximum projections of confocal stacks. Scale bars = 50 µm.

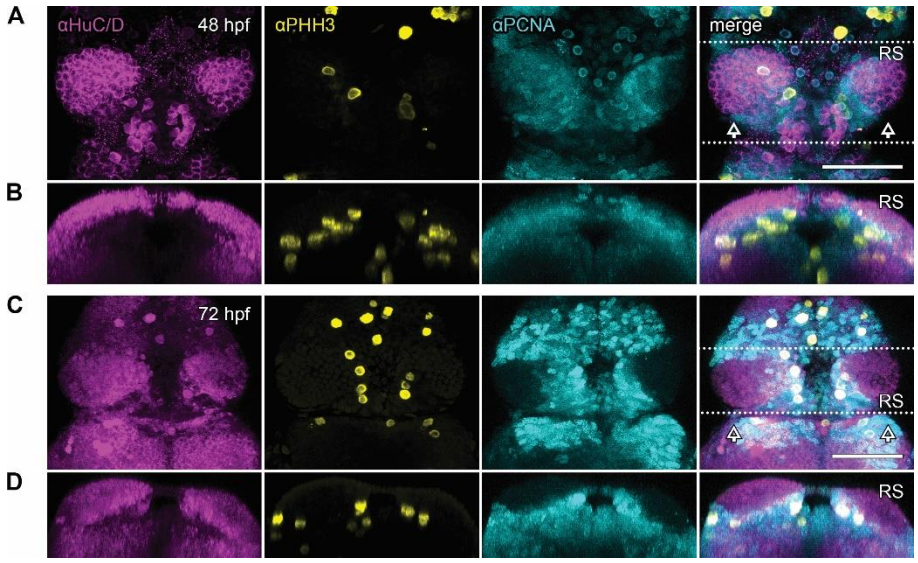

Fig. S7. The periventricular domain ventral to the pineal complex is proliferative. (**A-D**) Dorsal (A, C) and transverse projections (B, D) of 48 hpf (A, B) and 72 hpf (C, D) embryos stained with anti-HuC/D to mark differentiated neurons (magenta), anti-phospho-histone H3 to mark neuronal cells in M-phase (yellow) and anti-PCNA to mark neuronal cells in G1/S phase (cyan) of the cell cycle. Maximum projections of confocal stacks. The positions of habenulae are indicated with open arrowheads. The dotted lines in (A, C) indicate the volume shown in the transverse projections (B, D). Note that staining with anti-PCNA required antigen retrieval steps that inhibited anti-Cachd1 labelling, preventing co-staining; compare to Cachd1 expression in Fig. 1, S1, S2, S6. Scale bars = 50 µm.

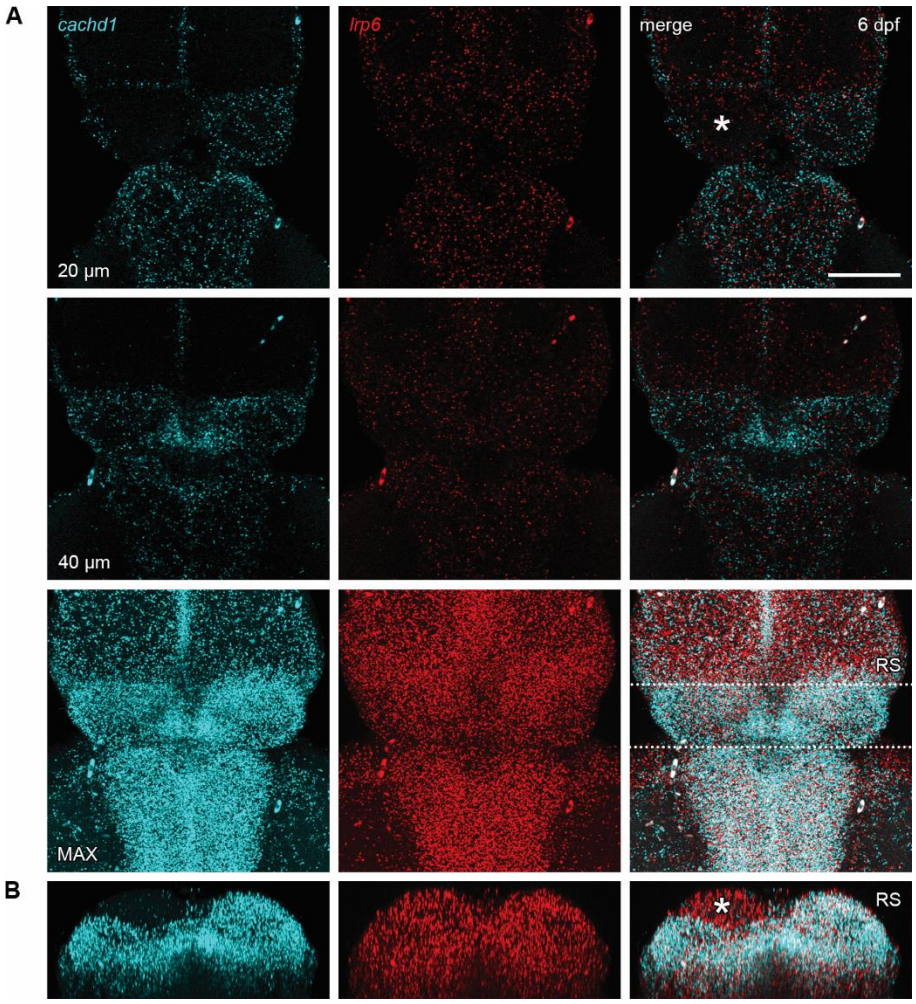

Fig. S8. Expression of *cachd1* is asymmetric at larval stages.
(**A**-**B**) Dorsal view (A) and transverse projection (B) of a dissected 6 dpf wildtype larva after *in situ* hybridization chain reaction with probes against *cachd1* (cyan) and *lrp6* (red).
(A) Single confocal slices at ~20 µm and 40 µm depth (from dorsal brain surface) and a maximum projection of the same confocal stack. Dotted lines indicate the approximate volume presented in the transverse projection (RS, B). *cachd1* expression remains in the periventricular habenular domain ventral to the pineal but is also expressed in the right habenula in its entirety; it is absent from the dorsal-most domain of the left dorsal habenula (asterisk). *lrp6* is expressed ubiquitously. Scale bar = 50 µm.

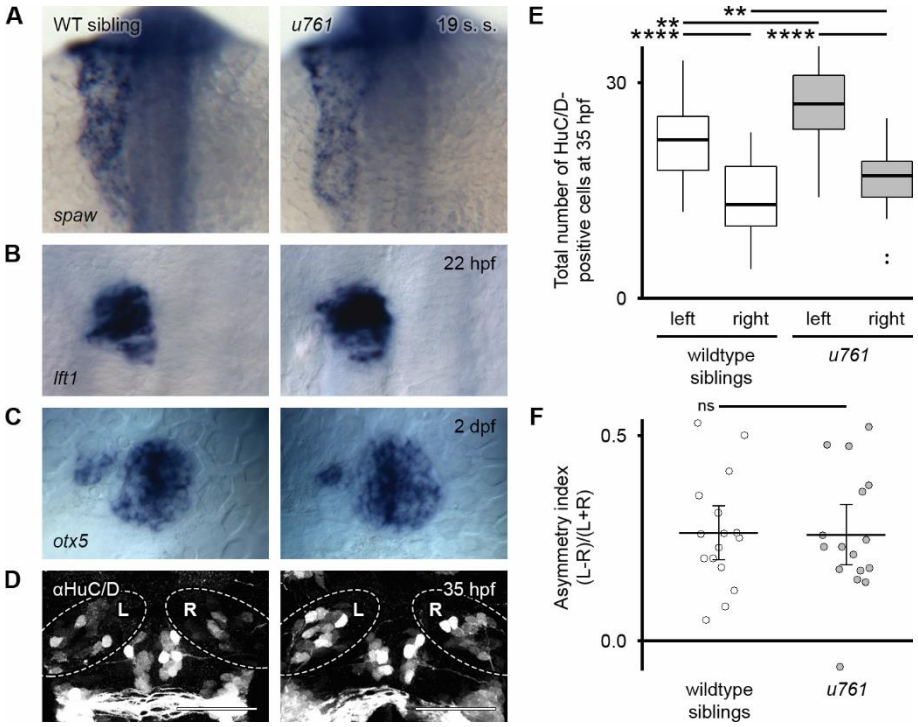

Fig. S9. Early Nodal-related left-right asymmetries are unperturbed in *cachd1*^{u761} mutants. (**A-C**) Dorsal views of wildtype sibling and *cachd1*^{u761} mutant embryos after colorimetric wholemount *in situ* hybridization with antisense riboprobes for the *nodal* signaling pathway ligand-encoding gene *spaw* (A, 19 somite stage) or target, *lft1* (B, 22 hpf), or pan-pineal complex marker *otx5* (C, 2 dpf) indicating early asymmetric expression of these marker genes is unaffected in *cachd1*^{u761} mutants. (**D**) Dorsal views of wildtype or *cachd1*^{u761} mutant embryos stained with anti-HuC/D to mark differentiated neurons at 35 hpf. Left and right dorsal habenula indicated with dotted lines. Note the overall increase in the number of differentiated neurons in the left and right dorsal habenula of *cachd1*^{u761} mutants (quantified in E). Maximum projections of confocal stacks. Scale bars = 50 µm. (**E**) Boxplots showing quantification of the number of anti-HuC/D-positive nuclei in the left and right dorsal diencephalon of wildtype siblings (white) and *cachd1*^{u761} mutants (grey); n = 16 for both groups. Kruskal-Wallis rank sum test (degrees of freedom = 3, $\chi^2 = 27.21$, $P = 5.3 \times 10^{-6}$) and *post hoc* pairwise comparisons using Wilcoxon rank sum test with continuity correction and Benjamini-Hochberg correction for multiple testing, ** $0.05 \geq P > 0.01$, **** $P \leq 0.005$. (**F**) Dot plots of the asymmetry index calculated for each wildtype sibling and *cachd1*^{u761} mutant embryo, based on the number of anti-HuC/D-positive nuclei. Although there is an overall increase in early neurogenesis in *cachd1*^{u761} mutants, there is a leftward bias, consistent with correct early Nodal-related asymmetry determination. Bar indicates sample mean and error bars indicate 95% confidence intervals of the mean. Welch two sample, two-tailed, *t*-test (degrees of freedom = 29.629, $t = 0.094$, $P = 0.926$), 'ns' $P > 0.1$.

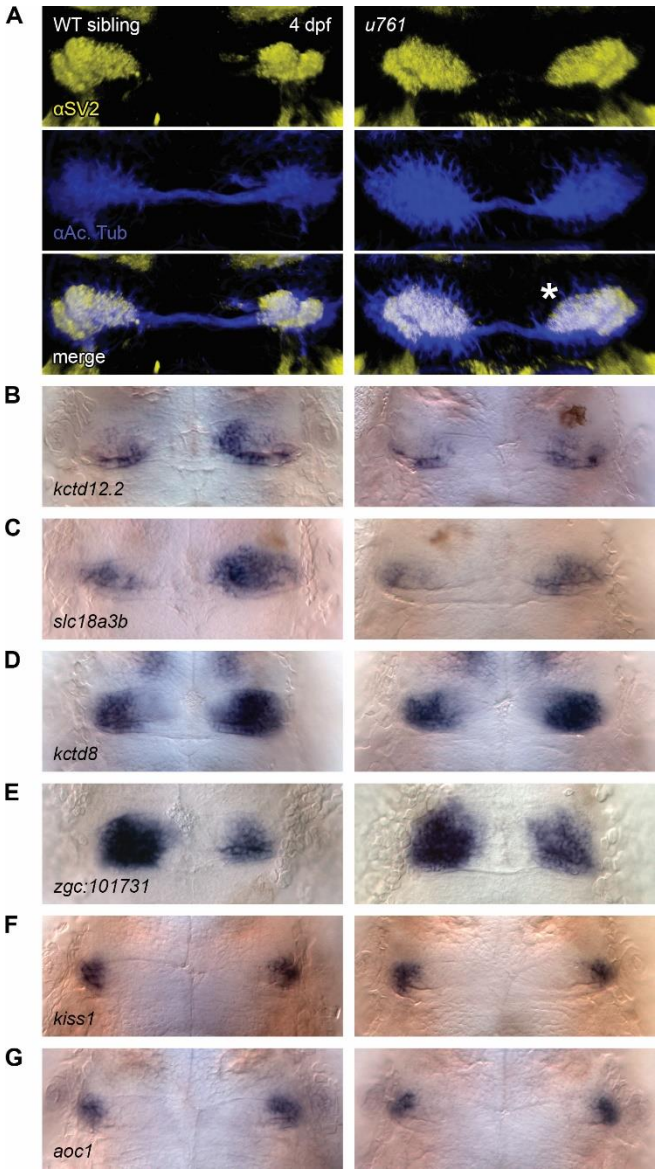

Fig. S10. Symmetric neuroanatomy and gene expression in the dorsal habenulae of *cachd1*^{u761} mutants.
(**A**) Dorsal views of immunohistochemistry labelling neuropil (anti-SV2, yellow) and axons (anti-acetylated tubulin, blue) in the habenulae in 4 dpf wildtype and *cachd1*^{u761} mutant larvae. Asterisk marks the increased volume of dHb$_L$-associated neuropil in the right habenula of *cachd1*^{u761} mutants. Maximum projections of confocal stacks. (**B**-**G**) Dorsal views of 4 dpf wildtype and *cachd1*^{u761} larvae after colorimetric wholemount *in situ* hybridization with riboprobes against dorsal habenula markers *kctd12.2* (B), *slc18a3b* (C), *kctd8* (D), *zgc*:101731 (E) and ventral habenula markers *kiss1* (F) and *aoc1* (G). The asymmetric dorsal habenula markers are reduced or symmetric in *cachd1*^{u761} mutants, but the ventral habenula markers are unaffected, suggesting *cachd1* does not play a role in neurogenesis of the ventral habenula.

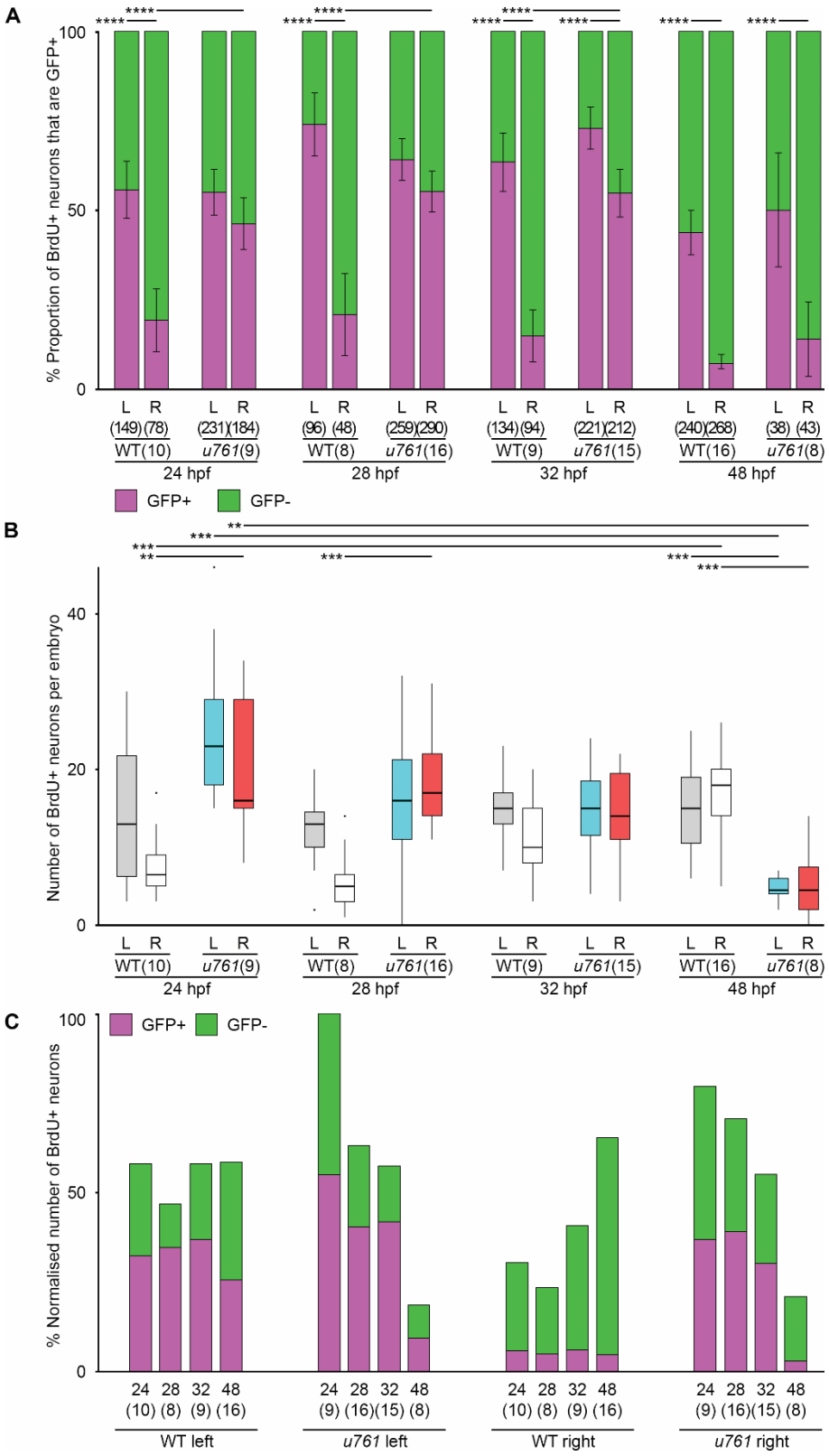

Fig. S11. Precocious neurogenesis in *cachd1*^{u761} mutant embryos with increased likelihood of acquiring lateral fate.

(**A**) Bar chart showing the proportion of BrdU-positive cells that express the dHb_L marker transgene *pku588Et* (GFP+, magenta) in 5 dpf wildtype sibling and *cachd1*^{u761} mutants given a pulse of BrdU at different stages (24 hpf – 48 hpf). Note the change in proportion in the right habenula of *cachd1*^{u761} mutants, indicating an increased likelihood of acquiring dHb_L character. Error bars represent 95% confidence intervals of the proportion, calculated using a normal approximation, or Wilson score when the proportion was less than 0.1, and/or the number of larvae tested was less than 20. The total number of cells and larvae in each condition is indicated in brackets. Samples for 24 hpf are replicated from Fig. 2 for comparison. Q′ test of equality of proportions within each BrdU pulse timepoint only (degrees of freedom = 3; 24 hpf: $\chi^2 = 40.94$, $P = 6.7 \times 10^{-9}$; 28 hpf: $\chi^2 = 16.44$, $P = 9.2 \times 10^{-4}$; 32 hpf: $\chi^2 = 24.20$, $P = 2.3 \times 10^{-5}$; 48 hpf: $\chi^2 = 50.70$, $P = 5.7 \times 10^{-11}$) and *post hoc* pairwise comparisons using a modified Marascuilo procedure with Benjamini-Hochberg correction for multiple testing, * $0.1 \geq P > 0.05$, ** $0.05 \geq P > 0.01$, **** $P \leq 0.005$. (**B**) Boxplot showing the number of BrdU-positive cells in the habenulae of 5 dpf wildtype sibling (grey left, white right) and *cachd1*^{u761} mutants (cyan left, red right) given a pulse of BrdU at different stages (24 hpf – 48 hpf). Note the substantial increase in neurogenesis at early stages and decrease at later stages in *cachd1*^{u761} mutants. Although differences in neurogenesis between left and right habenulae in wildtype embryos were too small to detect with statistical significance in this study (for example, 28 hpf L vs R: $P = 0.1066$), an increase in neurogenesis in the right habenula was observed between 24 hpf and 48 hpf timepoints (24 hpf WT R vs 48 hpf WT R: $P = 0.0052$). The number of larvae in each condition is indicated in brackets. Kruskal-Wallis rank sum test (degrees of freedom = 15, $\chi^2 = 70.98$, $P = 3.0 \times 10^{-9}$) and *post hoc* pairwise comparisons using Wilcoxon rank sum test with continuity correction and Benjamini-Hochberg correction for multiple testing, * $0.1 \geq P > 0.05$, ** $0.05 \geq P > 0.01$, *** $0.01 \geq P > 0.005$, **** $P \leq 0.005$. A limited number of significant differences are presented here for clarity. (**C**) Summary bar chart showing the total number of BrdU-positive neurons observed in the habenula of 5 dpf in a wildtype and *cachd1*^{u761} mutant larvae labelled at each BrdU pulse timepoint that were expressing the dHb_L marker transgene *pku588Et* (GFP+, magenta) or not (GFP-, green), normalized to the highest number of observed labelled neurons and the number of larvae in each condition. Note for example, the increased proportion of GFP+ neurons born on the right-hand side of *cachd1*^{u761} mutants at early stages compared to WT (significant differences identified in A) and the increased total number of neurons (significant differences identified in B).

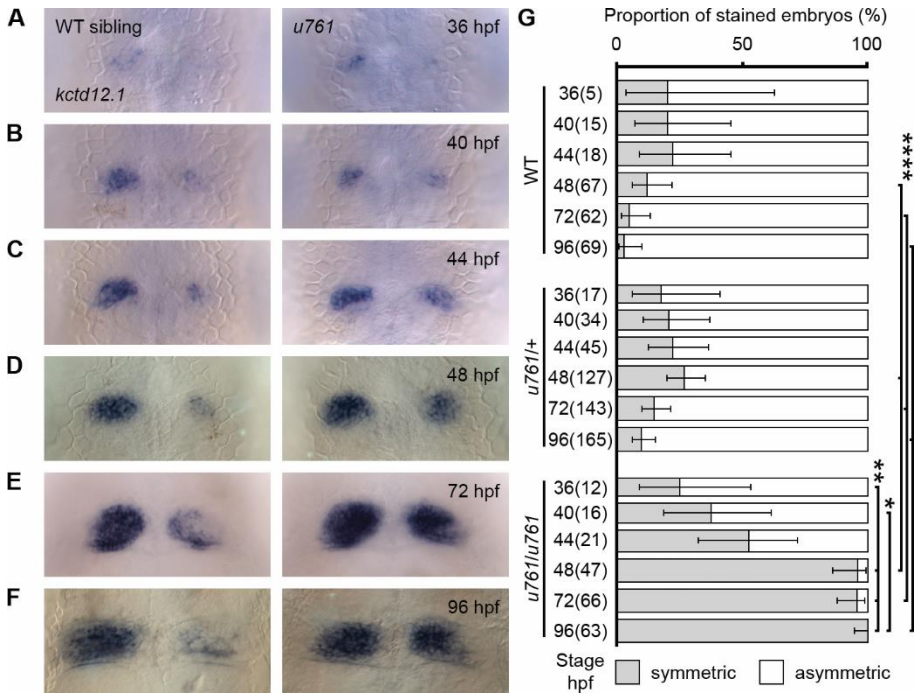

Fig. S12. Biased acquisition of left-sided character in right dorsal habenula of *cachd1*^{u761} mutants.

(**A-F**) Dorsal views of wildtype sibling and *cachd1*^{u761} mutant embryos at different developmental stages, 36 hpf (A) to 96 hpf (F), after colorimetric wholemount *in situ* hybridization with an antisense riboprobe for the dHb$_L$ marker *kctd12.1*. Expression of *kctd12.1* is increased in the right habenula of *cachd1*^{u761} mutants over the time course, consistent with an increased likelihood of acquiring dHb$_L$ fate. (**G**) Bar chart showing the proportion of wildtype, *u761/+* and *u761/u761* mutant embryos that showed symmetric (grey) or overtly asymmetric (white) *kctd12.1* staining at the different stages. Error bars represent the 95% confidence intervals for the proportion calculated using the Wilson score. Number of embryos in each condition is indicated in brackets. Q′ test of equality of proportions (degrees of freedom = 17, χ^2 = 646.41, $P = 2.1 \times 10^{-126}$) and *post hoc* modified Marascuilo procedure for multiple comparisons of proportions with Benjamini-Hochberg correction for multiple testing was used to test significance, ** $0.05 \geq P > 0.01$, **** $P \leq 0.005$.

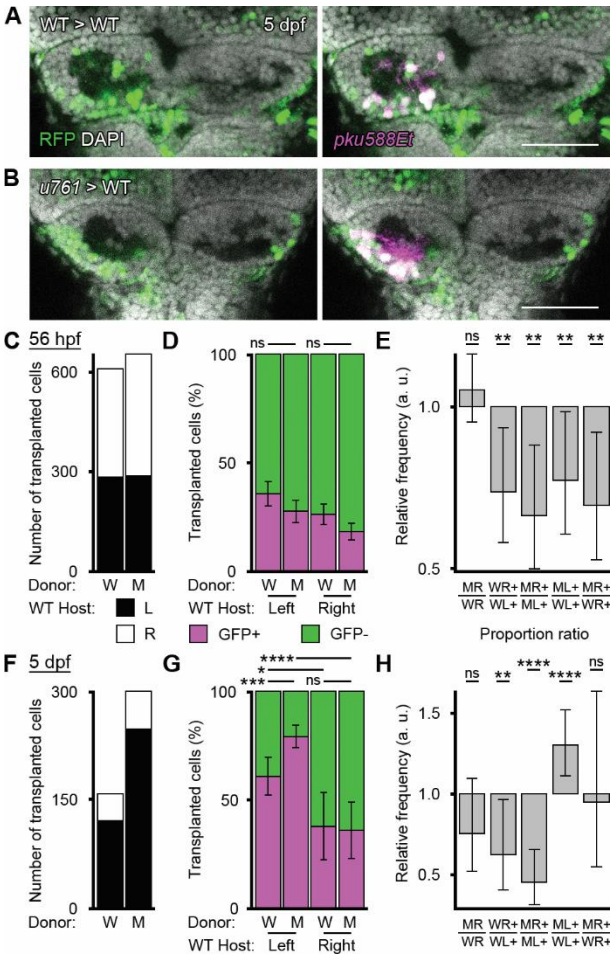

Fig. S13. Transplant experiments suggest that the loss of Cachd1 function does not have solely cell/lineage-autonomous consequences.
(**A**, **B**) Dorsal views of the habenulae of 5 dpf wildtype embryo hosts containing transplanted *pku588Et*, wildtype (A) or *u761* mutant (B) cells marked by expressing an RFP tracer (green). Expression of the *pku588Et* transgene (magenta) is specific to dHb_L cell types. Maximum projections of confocal stacks. Scale bars = 50 μm. (**C**, **F**) Charts showing the total number of transplanted *pku588Et*, wildtype (W) or *u761* mutant (M) cells counted in the left (black) or right (white) dorsal habenulae of 56 hpf (C) or 5 dpf (F) wildtype hosts (C: n = 25 (W), 31 (M); F: n = 4 (W), 12 (M)). (**D**, **G**) Charts showing the proportion of wildtype (W) or *u761* mutant (M) transplanted cells that express dHb_L-specific *pku588Et* (GFP+) in the left and right dorsal habenula of 56 hpf (D) or 5 dpf (G) WT hosts. Error bars represent the 95% confidence interval of the proportion. Q′ test of equality of proportions (D: degrees of freedom = 3, $\chi^2 = 21.04$, $P = 1.0 \times 10^{-4}$; G: degrees of freedom = 3, $\chi^2 = 48.47$, $P = 1.7 \times 10^{-10}$) and *post hoc* modified Marascuilo procedure with Benjamini & Hochberg correction for multiple testing. Only comparisons within transplant genotype or within position in host are shown for clarity. (**E**, **H**) Charts showing the relative frequency (risk) ratios of different proportions in the transplant data from 56 hpf (E) or 5 dpf (H) wildtype hosts. A value of 1 indicates equality of the proportions. Error bars represent the 95% confidence interval of the relative frequency. Fisher's exact test with Benjamini-Hochberg correction for multiple testing. Note that there was an equal likelihood of a transplanted cell being observed in the left or right dorsal habenula regardless of genotype at both timepoints ($\hat{p}_{MR} \approx \hat{p}_{WR}$), although there were fewer transplanted cells on the right than left

at 5 dpf. The likelihood of *pku588Et* expression was also asymmetric between left and right dorsal habenula for both wildtype and *u761* mutant cells at both timepoints ($\hat{p}_{WL+} > \hat{p}_{WR+}$ and $\hat{p}_{ML+} > \hat{p}_{MR+}$). At 56 hpf, the likelihood of a *u761* mutant transplant cell expressing *pku588Et* was reduced compared to wildtype cells on either side of the epithalamus ($\hat{p}_{WL+} > \hat{p}_{ML+}$ and $\hat{p}_{WR+} > \hat{p}_{MR+}$). However, at 5 dpf, *u761* mutant transplant cells were more likely to express *pku588Et* than wildtype cells in the left habenula ($\hat{p}_{WL+} < \hat{p}_{ML+}$) but equally likely in the right habenula ($\hat{p}_{WR+} \approx \hat{p}_{MR+}$). This suggests that the *u761* allele does not have strictly cell autonomous consequences on selection of subtype identity and that the environments of the left and right habenula are not equivalent. 'ns' $P > 0.1$, * $0.1 \geq P > 0.05$, ** $0.05 \geq P > 0.01$, *** $0.01 \geq P > 0.005$, **** $P \leq 0.005$.

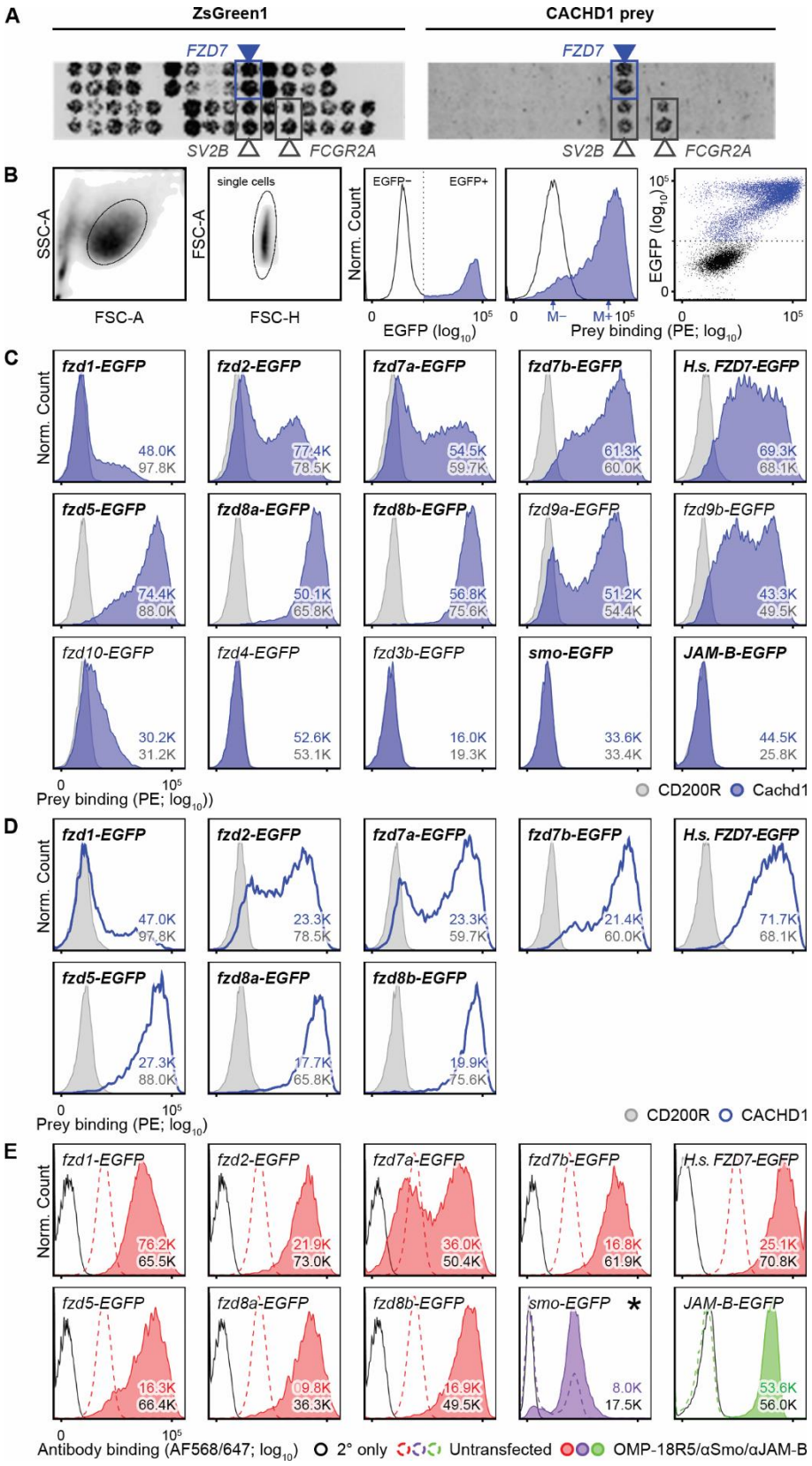

Fig. S14. Physical interactions of Cachd1 with Fzd family proteins detected by cell microarray and flow cytometry.

(**A**) Cell microarray data showing the interaction between a human CACHD1 prey protein and its target FZD7 (blue). Expression vectors encoding both ZsGreen1 and FZD7, together with a range of interactions from alternative prey proteins were spotted onto slides, and human HEK293 cells were reverse transfected. Fixed cells were subsequently incubated with human CACHD1 prey protein and detected with an AlexaFluor-647 conjugated secondary antibody. ZsGreen fluorescence was used to confirm transfection efficiency and spot locations on the slides (left-hand panel). Two other hits, SV2B and FCGR2A, were considered false positives because of multiple binding interactions with a wide range of prey proteins. (**B**) Gating strategy for testing specific interactions with transiently transfected cells. Single cells were isolated by forward (FSC-A, FSC-H) and side (SSC-A) light scatter, then separated into EGFP-negative (untransfected or not expressing the EGFP fusion protein bait; black outline) and EGFP-positive (transfected, blue) gates. Prey binding is indicated by increased PE fluorescence in the EGFP-positive population. The ratio of median PE fluorescence of either subpopulation ($\Delta M_{PE} = \ln(M_{PE}^{EGFP+}/M_{PE}^{EGFP-})$) was used to quantify the degree of prey binding to the EGFP-positive population. (**C**, **D**) Examples of normalized histograms of EGFP-positive populations for each EGFP fusion protein bait transfection indicated, tested with either zebrafish Cachd1 (C, solid blue), human CACHD1 (D, blue outline) or CD200R negative control prey (grey). Note that human CACHD1 prey is able to bind zebrafish Fzd family proteins and *vice versa*, suggesting conservation of binding (not all combinations tested). Numbers in each panel indicate the total number of EGFP-positive events collected for each condition over all replicates. Bold transfection titles indicate validation of surface expression with antibodies. (**E**) Examples of normalized histograms of EGFP-positive populations for each EGFP fusion protein bait tested with antibodies to detect surface expression of Fzd family proteins (OMP-18R5, red), Smo-EGFP (purple) or negative control bait protein JAM-B-EGFP (green). The dotted line in each panel indicates antibody binding fluorescence in mock transfected HEK293E cells; black outline indicates the secondary only negative control. Note that untransfected HEK293E cells appear to have endogenous surface expression of Fzd family receptor(s) and the Smo receptor (dotted lines). Numbers in each panel indicate the total number of EGFP-positive events collected for each condition. Asterisk indicates a formaldehyde-fixed cell population.

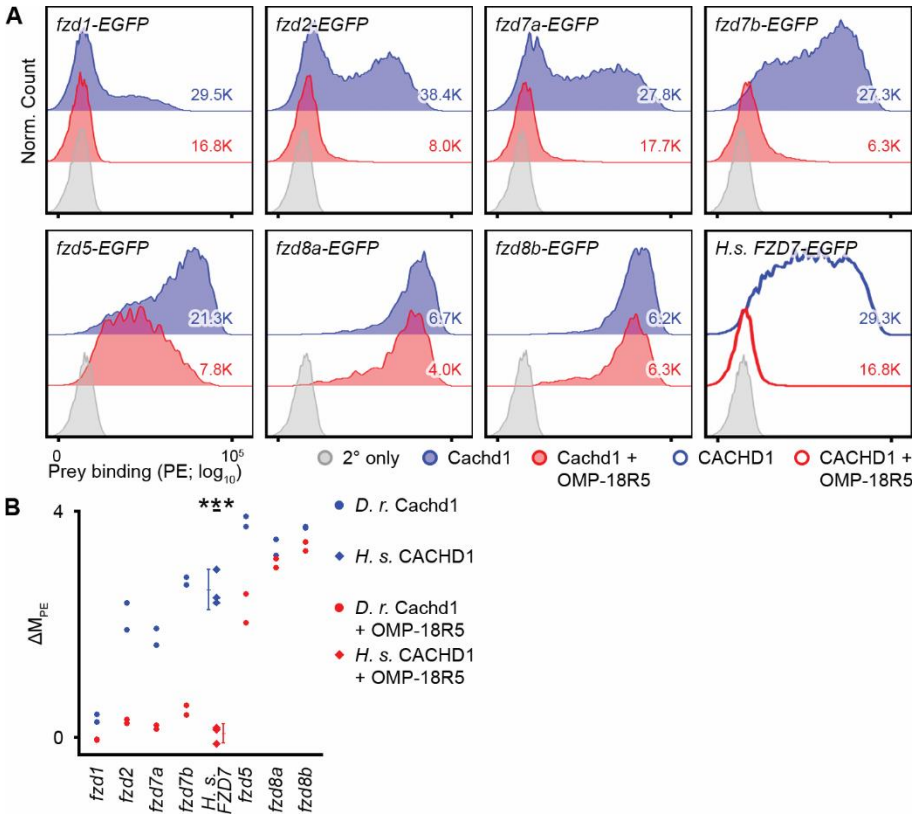

Fig. S15. Cachd1 prey binding to Fzd family receptors blocked by anti-Fzd antibody. (**A**) Examples of normalized histograms of EGFP-positive populations for each EGFP fusion protein bait transfection indicated, tested with either zebrafish Cachd1 prey protein alone (blue) or after pre-incubation of the cells with OMP-18R5 antibody (red). Human FZD7-EGFP histogram duplicated from Fig. 3A for comparison. Secondary antibody only control shown in grey. Total number of events collected for each condition indicated in each plot. Note that Cachd1 prey binding to zebrafish Fzd family bait proteins Fzd1/2/7a/7b is effectively blocked by OMP-18R5 pre-incubation, but not to Fzd5/8a/8b. (**B**) Dot plot showing ΔM_{PE} for transfections tested for Cachd1 prey protein interaction (circles and diamonds represent zebrafish and human prey proteins respectively) with (red) or without pre-incubation with OMP-18R5 (blue). Mean indicated with a single line, error bars indicate 95% confidence intervals of the mean. One-tailed paired *t*-test for human CACHD1-FZD7 interaction only (degrees of freedom = 2, $t = 9.53$, *** $P = 0.0054$), due to limited numbers of replicates for other inhibition tests.

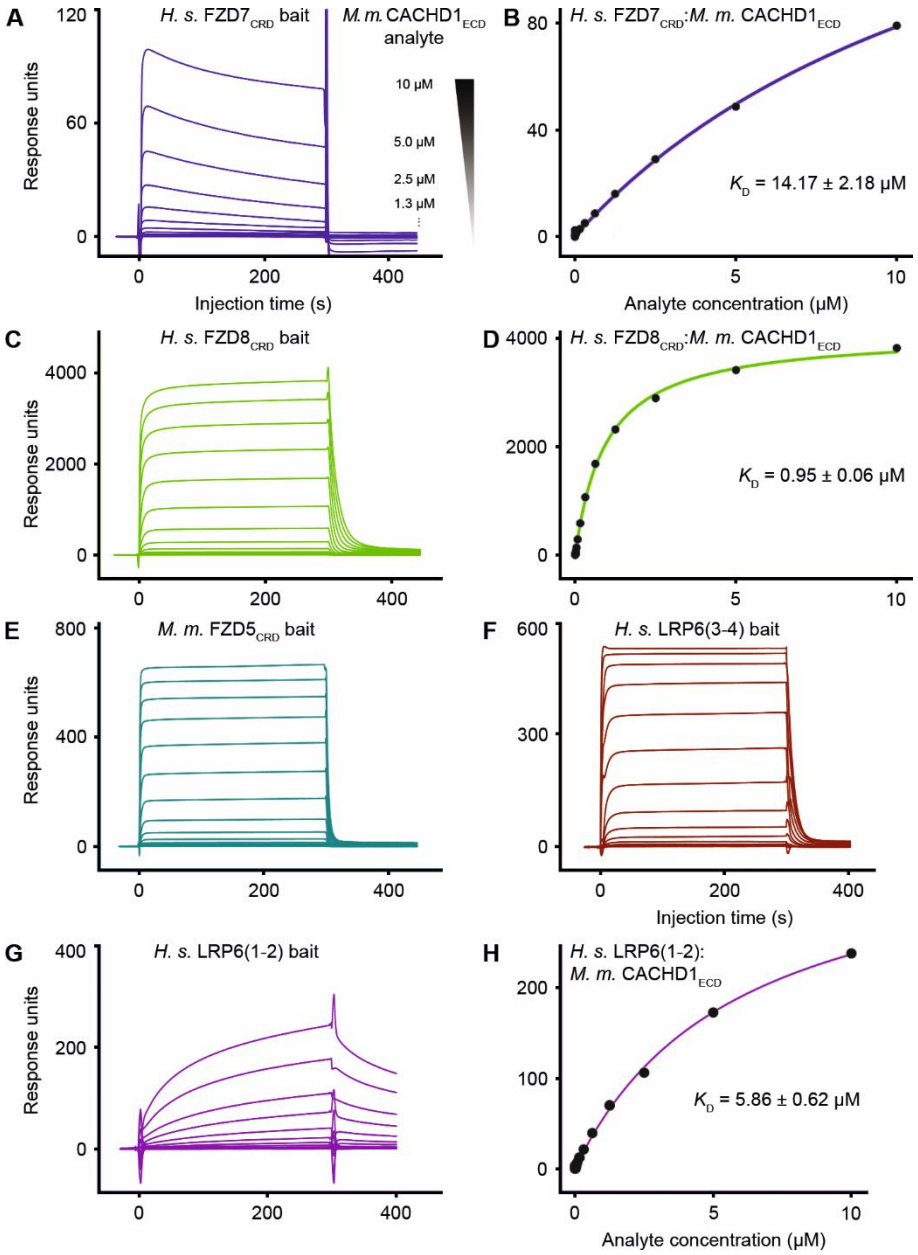

Fig. S16. SPR analysis of CACHD1$_{ECD}$ interactions with LRP6 and FZD$_{CRD}$ domains. (**A**, **C**, **E-G**) Surface plasmon resonance sensorgrams showing the response of different concentrations of mouse CACHD1$_{ECD}$ analyte flowing over surfaces of immobilized human FZD7$_{CRD}$ (A), human FZD8$_{CRD}$ (C), mouse FZD5$_{CRD}$ (E), human LRP6$_{P3E3P4E4}$ (3-4, F), and LRP6$_{P1E1P2E2}$ (1-2, G). (**B**, **D** and **H**) Graphs showing the determination of the equilibrium constants (K_D ± 95% C.I.) for those interactions, except for FZD5$_{CRD}$ and LRP6$_{P3E3P4E4}$ which are shown in Figure 3.

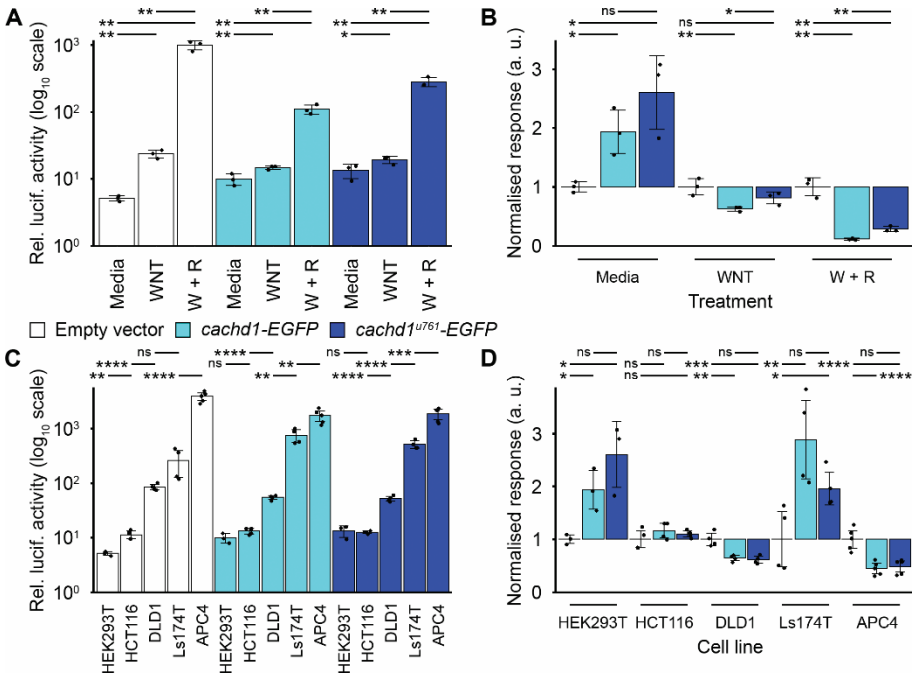

Fig. S17. Overexpression of Cachd1 strongly antagonizes RSPONDIN1-based sensitivity to canonical Wnt signaling and modulates pathway activity.
(**A**-**D**) Summary charts of TOP-FLASH assays performed in HEK293T (A and B) and cancer cell lines (C and D, HEK293T data from B replicated for comparison) transfected with zebrafish *cachd1-EGFP* (cyan), *cachd1*^{u761}*-EGFP* (dark blue) or empty vector control (white). (A) Mean relative luciferase responses ($\log_{10}$ scale) of transfected HEK293T cells after treatment with media alone (Media), WNT3A-conditioned media (WNT) or WNT3A and RSPONDIN1-condition media (W + R). (B) Responses in (A) normalized to the empty vector control for each treatment. (C) Mean relative luciferase responses ($\log_{10}$ scale) of transfected HEK293T and Wnt pathway mutant cancer cell lines HCT116, DLD1, Ls174T and APC4, in media alone. (D) Responses in (C) normalized to the empty vector control for each cell type. Note that transfection of cells with the *cachd1*^{u761} mutant construct also elicited effects on canonical Wnt signaling responses, to a lesser degree than wildtype. This is most likely an overexpression artefact, as high expression leads to the presence of mutant Cachd1 protein on the cell surface (see Fig. S1A). Individual points represent the mean response of an individual experiment, calculated from at least triplicate measurements, and error bars indicate 95% confidence intervals of the mean. One way Welch test of means were performed on raw response data (not assuming equal variances; A: $F = 53.25$, D. $F_{num} = 8.00$, D. $F_{denom} = 7.05$, $P = 1.3 \times 10^{-5}$; C: $F = 65.01$, D. $F_{num} = 14.00$, D. $F_{denom} = 16.33$, $P = 1.4 \times 10^{-11}$), *post hoc* pairwise *t*-tests with non-pooled standard deviations, Benjamini-Hochberg correction for multiple testing; only significant differences within transfection group (A, C), treatment group (B) or cell line (D) are presented here for clarity, 'ns' $P > 0.1$, * $0.1 \geq P > 0.05$, ** $0.05 \geq P > 0.01$, *** $0.01 \geq P > 0.005$, **** $P \leq 0.005$.

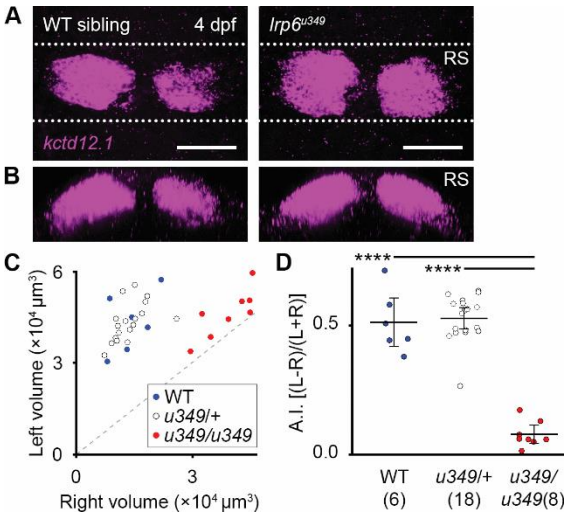

Fig. S18. Quantification of *lrp6* mutant phenotype.
(**A, B**) Dorsal (A) and (B) transverse projection of 4 dpf wildtype sibling and *lrp6*^{u349} mutant larvae after fluorescent RNA *in situ* hybridization with riboprobes against *kctd12.1*. Maximum projections of confocal stacks. Dotted lines represent the approximate volume in the transverse projections (RS, B). Scale bars = 50 µm. (**C**) Scatterplot showing quantification of *kctd12.1*-fluorescent volumes in the left and right habenulae of wildtype (blue), *u349/+* (white) and *u349/u349* (red) siblings at 4 dpf, represented with a single point. The grey dashed line represents the line of symmetry between left and right volumes. Note the increase in the volume of *kctd12.1* in the right habenula of *lrp6*^{u349} mutants compared to wildtype or heterozygous siblings. (**D**) Dot plot showing the asymmetry index calculated using *kctd12.1* volumes for each wildtype, *u349/+* and *u349/u349* sibling larvae. Mean asymmetry index for each genotype is indicated with a horizontal bar. Error bars represent 95% confidence intervals of the mean. Number of larvae for each condition indicated in brackets. Wildtype and *lrp6*^{u349} heterozygous siblings have leftward asymmetry of the *kctd12.1* marker, but the increase in right habenula volume renders *lrp6*^{u349} mutants symmetric. ANOVA (degrees of freedom = 2, $F = 77.34$, $P = 2.4 \times 10^{-12}$) and *post hoc* Tukey pairwise comparisons were used for hypothesis testing, **** $P \leq 0.005$.

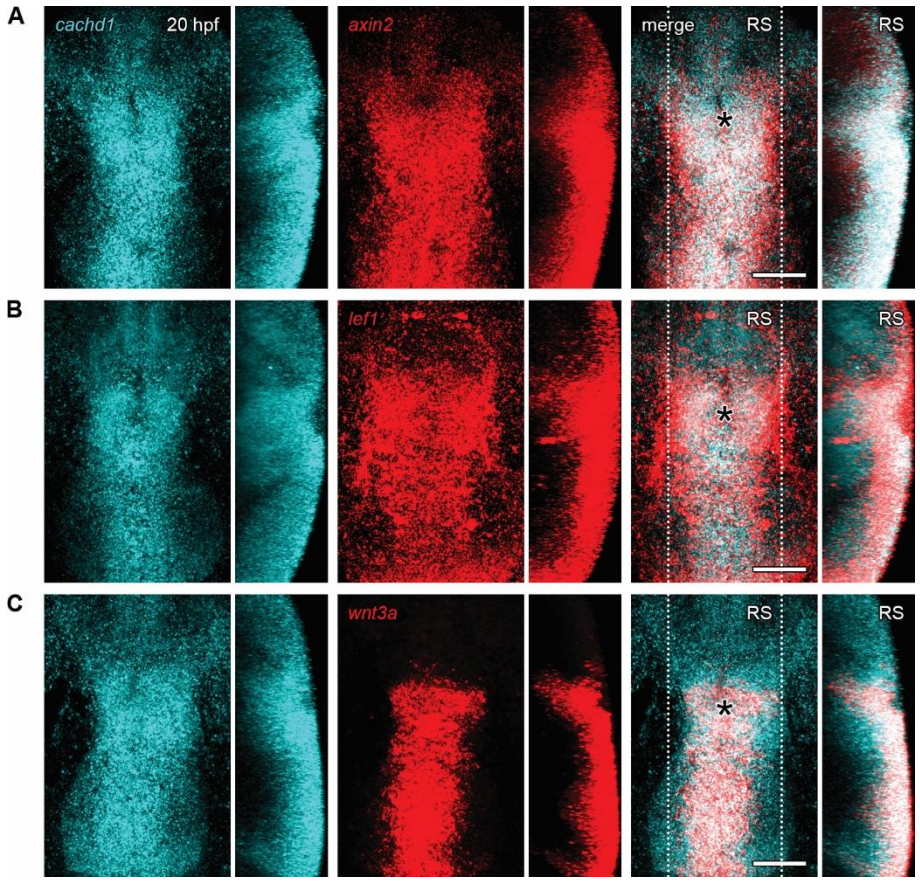

Fig. S19. *cachd1* is co-expressed with other Wnt pathway genes in the dorsal diencephalon and midbrain roof plate.
(**A**-**C**) Dorsal views (left panels) and sagittal projections (RS, right panels) of 20 hpf wildtype embryos after double fluorescent *in situ* hybridization staining with antisense riboprobes for *cachd1* (cyan) and Wnt pathway genes *axin2* (A, red), *lef1* (B, red) or *wnt3a* (C, red) showing *cachd1* is expressed in Wnt active tissues in early development. The approximate position of the pineal is marked with an asterisk. Maximum projections of confocal stacks. Dotted lines represent the approximate volume shown in the sagittal projections (RS). Scale bars = 50 µm.

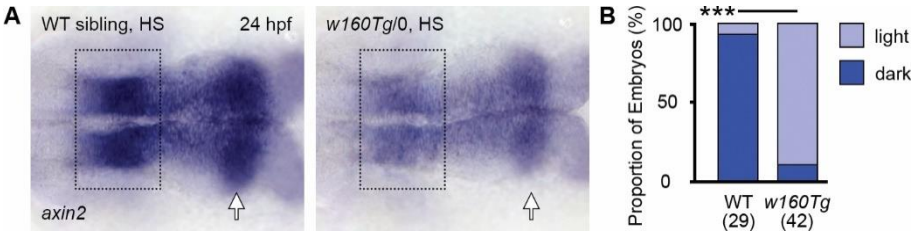

Fig. S20. Heat shock induction of Cachd1 reduces expression of *axin2*.
(**A**) Representative dorsal views of flat mounted wildtype (left) and *Tg(HSE:cachd1, EGFP)w160* (right) 24 hpf embryos, heat shocked at 18-20 somites stage, after *in situ* hybridization with an *axin2* riboprobe (anterior left). The dorsal diencephalon is indicated with a dotted box and the midbrain-hindbrain boundary with a white arrow. Note the decrease in staining intensity in the *w160Tg* hemizygote embryos. (**B**) Chart showing the proportion of heat shocked embryos with dark or light *axin2* staining (subjectively assessed). Numbers in brackets indicate the total number of embryos tested. Fisher's exact test, *** $P < 0.01$.

Table S1. Cross validation of anti-Cachd1 antibody and *cachd1* null allele.

Genotype	IHC Staining Intensity			Total
	High	Low	Absent	
wildtype	11	2	0	13
sa17010/+	0	19	0	19
sa17010/*sa17010*	0	1	10	11
n. d.	0	1	0	1
Total	11	23	10	44

Fisher's exact test: $P = 4.0 \times 10^{-7}$

Table S2. Data collection and refinement statistics for the CACHD1$_{ECD}$:FZD5$_{CRD}$:LRP6$_{P3E3P4E4}$ ternary complex (PDB:8S7C).

Data collection		Refinement	
Source	Diamond I03	Resolution (Å)	72.33-4.72
Wavelength(Å)	0.9762	No. unique reflections	23489(154)
Space group	$C2_1$	R_{work} / R_{free}	0.196/0.243
Cell dimensions:		No. atoms:	41757
a, b, c (Å)	283.70, 198.24, 218.82	Protein	41211
α, β, γ (°)	90, 128.08, 90	Ligand/ion	546
Resolution (Å)	172.26-4.72(4.87) *	Water	0
R_{sym} or R_{merge}	0.24(---)	*B*-factors:	
I / σI	6.3(1.6)	Protein	211.42
Completeness (%)	88.8(68.0)	Ligand/ion	216.30
Redundancy	6.8(7.0)	Water	n/a
CC(1/2)	0.99(0.44)	R. m. s. deviations:	
		Bond lengths (Å)	0.004
		Bond angles (°)	0.86

* Values in parentheses are for highest-resolution shell.

Table S3. Allelic series of *lrp6* nonsense mutations show a bilateral 'double left' phenotype.

lrp6 allele number	Genomic lesion (Zv11 assembly)	Freq. of double left phenotype*				χ^2 (2 d. o. f.)	*P* value
		WT	+/-	-/-	Total		
u348	11 bp del. + 9 bp del. (4:76249-76259del; 76390-76398del, p.L45RfsX28)	0/27	2/44	27/29	100	81.7	1.8×10^{-18}
u349	4 bp ins. (4:76250-76251insATGG, p.V46MfsX32)	0/17	0/55	18/19	91	n. a. †	8.0×10^{-18}
u350	23 bp del. (4:76390-76412del, p.V92GfsX11)	0/25	0/46	26/27	98	93.1	6.2×10^{-21}
u351	149 bp del. + 9 bp ins. (4:76242-76390del; insCACGCCACG, p.A43HfsX21)	0/12	0/16	9/9	37	n. a. †	8.0×10^{-9}

* assessed by colorimetric *in situ* hybridisation with *kctd12.1* riboprobe

† Fisher's exact test was used where expected values were below 5

Table S4. Oligonucleotides for generating CRISPR/Cas9 sgRNAs targeting *lrp6* exon 2.

Gene	Guide	Primer sequence (target sequence underlined in bold)
lrp6	sg1	GCGTAATACGACTCACTATA**GGCCAACGCCACGCTGGTGA**GTTTTAGAGC TAGAAATAGCAAG
lrp6	sg2	GCGTAATACGACTCACTATA**GGCCAGACCGGAGATGACGG**GTTTTAGAGC TAGAAATAGCAAG
Template oligo sequence:		AAAAGCACCGACTCGGTGCCACTTTTTCAAGTTGATAACGGA CTAGCCTTATTTTAACTTGCTATTTCTAGCTCTAAAAC

Table S5. Primer sequences used for mapping, genotyping, qPCR, headloop PCR and cloning.

Species	Gene	Name	Sequence
Zebrafish	*ak4*	e1-Mapping-F	CTGTTTTGCACCTCCAACCT
Zebrafish	*ak4*	e1-Mapping-R	GCTTCACGGAGCATATGACA
Zebrafish	*cachd1*	i8-9-Mapping-F	TTTCAACACTTTGGCCTGTT
Zebrafish	*cachd1*	i8-9-Mapping-R	GCAGTGCAGAAGAGGGTTTC
Zebrafish	*cachd1*	u761-AloI-F	TTTAACTGCACTGTTTTGCCTTA
Zebrafish	*cachd1*	u761-AloI-R	ATAGGCATAAACGGCGAACA
Zebrafish	*cachd1*	HRMA-sa17010-F	GAGCAATCTGGAGCTGGGTT
Zebrafish	*cachd1*	HRMA-sa17010-R	TGTATGTCGCGGCAGTAAGG
Zebrafish	*cachd1*	cloning-FL-SalI-F	ATGAACGTCGACTGCGAAACGGAAAAGTTAGG
Zebrafish	*cachd1*	cloning-FL-SacII-R	TGCAATCCGCGGGCACTCAGCGTCCACACT
Zebrafish	*cachd1*	RT-PCR-e1-F*	TGCGAAACGGAAAAGTTAGG
Zebrafish	*cachd1*	RT-PCR-e9-R	CCCACTGTGGTCTCCAGATT
Zebrafish	*cachd1*	RT-PCR-e8-F	CGCAGTGAAAGAGGAGAACC
Zebrafish	*cachd1*	RT-PCR-e17-R	CCGAATTTTGTTGCCTTTGT
Zebrafish	*cachd1*	RT-PCR-e16-F	CTGGACCGTACCTGGATGTT
Zebrafish	*cachd1*	RT-PCR-e27-R*	TGAGGGTTGGTTCTGAGGTC
Zebrafish	*lrp6*	CRISPR-sg1-HRMA-F	TGTGTTCCACTGGAGTGACATT
Zebrafish	*lrp6*	CRISPR-sg1-HRMA-R	CAGGCCCTGCGCATAGATATAA
Zebrafish	*lrp6*	CRISPR-sg2-HRMA-F	GATCTACTGGAGCGACGTGAG
Zebrafish	*lrp6*	CRISPR-sg2-HRMA-R	TCGGAGTCGGTCCAGTAAAGTT
Zebrafish	*lrp6*	HLPCR-control-F	AGATGTTTTGAAGAGTGCGGTG
Zebrafish	*lrp6*	HLPCR-control-R	TAAACATCCCGAAAACAAGCTGC
Zebrafish	*lrp6*	HLPCR-HL-sg1-F	CCATCACCAGCGTGGCGTTGAGATGTTTTGAAGAGTGCGGTG

Zebrafish	*lrp6*	HLPCR-HL-sg2-R	CACCGTCATCTCCGGTCTGGTAAACATCCCGAAAACAAGCTGC
Zebrafish	*slc18a3b*	riboprobe-cloning-F	GGAGAGCTCGTGCGTAATTC
Zebrafish	*slc18a3b*	riboprobe-cloning-R	CACTTAGAGGCGTCCATCGT
Zebrafish	*zgc:101731*	riboprobe-cloning-F	GGTGTTGAGCGAGAGTTGGT
Zebrafish	*zgc:101731*	riboprobe-cloning-R	TGTTTTCAAACCTTTGACTGG
Zebrafish	*aoc1*	riboprobe-cloning-F	ACAACGGGCAGTATTTCGAC
Zebrafish	*aoc1*	riboprobe-cloning-R	TTCTGTAGCGCACAGGTTTG
Zebrafish	*kiss1*	riboprobe-transcription-F	ATGCTGCTTACTGTCATATTGATG
Zebrafish	*kiss1*	riboprobe-T3-transcription-R	GGATCCATTAACCCTCACTAAAGGGACACCTAAAACATGAAGGCAAATACC
Zebrafish	*fzd1*	fusion-PCR-5'-F	TGGCCGACTGGAGACTCTTTC
Zebrafish	*fzd1*	fusion-PCR-5'-R	CACTGGAAGCGTCCGCGCTG
Zebrafish	*fzd1*	fusion-PCR-3'-F	CTCCCAGCGCGGACGCTTCC
Zebrafish	*fzd1*	fusion-PCR-3'-R	CGAAAGCAGAGCTTCACACTGTGG
Zebrafish	*fzd1*	cloning-NotI-F	GCGGCCGCCACCATGGCAGCTCGCGCTCTCTTC
Zebrafish	*fzd1*	cloning-AscI-R	GACTATGGCGCGCCCACTGTGGTTTCTCCCTGTTTGCTGTTCGCC
Zebrafish	*fzd2*	cloning-NotI-F	GCGGCCGCCACCATGGCAGCGAGTGGAAGTGTG
Zebrafish	*fzd2*	cloning-AscI-R	GAGTGAGGCGCGCCAACAGTGGTTTCTCCTTGTCC
Zebrafish	*fzd3b*	cloning-NotI-F	GCGGCCGCCACCATGGGCTGTGTTGTGGATTTACC
Zebrafish	*fzd3b*	cloning-AscI-R	TAGTATGGCGCGCCCGCACTGGTCCCGTTCTCCGG
Zebrafish	*fzd4*	cloning-NotI-F	GCGGCCGCCACCATGGCTCGGTTTGAGTTCGGG
Zebrafish	*fzd4*	cloning-AscI-R	TAGTTAGGCGCGCCCACAACCGTCTCGTTTCCTTTGCCCGG
Zebrafish	*fzd5*	cloning-NotI-F	GCGGCCGCCACCATGGGGAAACCTGCAGACGAG
Zebrafish	*fzd5*	cloning-AscI-R	GACGCTGGCGCGCCGACATGTGATGAGGGTGCTGATTTGTG

Zebrafish	*fzd7a*	cloning-NotI-F	GCGGCCGCCACCATGGCTTTCCTCAAGATGCAAC
Zebrafish	*fzd7a*	cloning-AscI-R	TAGTATGGCGCGCCTACCGTCGTCTCGCCCTGGT
Zebrafish	*fzd7b*	cloning-NotI-F	GCGGCCGCCACCATGGCGGTACGGGAAGTTGG
Zebrafish	*fzd7b*	cloning-AscI-R	GAGTGAGGCGCGCCCACCGTTGTTTCCCCTTGGTTG
Zebrafish	*fzd8a*	cloning-NotI-F	GCGGCCGCCACCATGGAGTGCTACCTGTTGGG
Zebrafish	*fzd8a*	cloning-AscI-R	TACTCTGGCGCGCCGACTTGGGACAAAGGCATCTGCTTGGG
Zebrafish	*fzd8b*	fusion-PCR-5'-F	CCAGAGCACATGCCAGCGCATCC
Zebrafish	*fzd8b*	fusion-PCR-5'-R	GTGCACAGGGCTCGCCAGGAATC
Zebrafish	*fzd8b*	fusion-PCR-3'-F	GATTCCTGGCGAGCCCTGTGCAC
Zebrafish	*fzd8b*	fusion-PCR-3'-R	TCATCACACACGAGAAAGTGGCATTTGTTTTGGAGG
Zebrafish	*fzd8b*	cloning-NotI-F	GCGGCCGCCACCATGGACTCGCCTACACACAGGG
Zebrafish	*fzd8b*	cloning-AscI-R	GACGCTGGCGCGCCCACACGAGAAAGTGGCATTTGTTTTGG
Zebrafish	*fzd9a*	cloning-NotI-F	GCGGCCGCCACCATGGGACATTGCATGAAGATTGGG
Zebrafish	*fzd9a*	cloning-AscI-R	TGATCGGGCGCGCCAACATGTGTGGGACTGTCTGTATAG
Zebrafish	*fzd9b*	cloning-NotI-F	GCGGCCGCCACCATGGGAAGCTCACCTCTGCAAATTG
Zebrafish	*fzd9b*	cloning-AscI-R	TAGCTCGGCGCGCCTACATGTGTGGGACAGTCTGAGTAGG
Zebrafish	*fzd10*	cloning-NotI-F	GCGGCCGCCACCATGGTTGCTGCCGGTGTCGG
Zebrafish	*fzd10*	cloning-AscI-R	GAGCGTGGCGCGCCTACACAAGTTGCAGGAGGACCTGCTG
Zebrafish	*smo*	cloning-NotI-F	GCGGCCGCCACCATGTCCTCCAAGCGCCCCTGCTCCATT
Zebrafish	*smo*	cloning-AscI-R	TGCGCAGGCGCGCCAAAATCTGAGTCAGCATCCAATAGCTCAGC

Zebrafish	*gng8*	cloning-PCR-F	CATCATACTAGTGGGCTATAAAACAAAATG
Zebrafish	*gng8*	cloning-PCR-R	CATCATGATATCTTCGTTTGTAGAGACCAA
Mouse	*Cachd1*	qPCR-F	AGTTCAGCAGCTAGCCAAAAA
Mouse	*Cachd1*	qPCR-R	CCATCAAACTCCATCATGGA
Mouse	*Ccnd1*	qPCR-F	GCCATCCAAACTGAGGAAAA
Mouse	*Ccnd1*	qPCR-R	GATCCTGGGAGTCATCGGTA
Mouse	*Axin2*	qPCR-F	TCCAGAGAGAGATGCATCGC
Mouse	*Axin2*	qPCR-R	AGCCGCTCCTCCAGACTATG
Mouse	*Hprt1*	qPCR-F	TCATGAAGGAGATGGGAGGC
Mouse	*Hprt1*	qPCR-R	CCACCAATAACTTTTATGTCCCC
Human	*CACHD1*	qPCR-F	CTTAAATTCAGTTCTTGCAG
Human	*CACHD1*	qPCR-R	CGTAGATGGGTCTACTGCGG
Human	*CCND1*	qPCR-F	CTCCGCCTCTGGCATTTTGG
Human	*CCND1*	qPCR-R	TCTCCTTGCAGCTGCTTAG
Human	*AXIN2*	qPCR-F	AGTGTGAGGTCCACGGAAAC
Human	*AXIN2*	qPCR-R	CTTCACACTGCGATGCATTT
Human	*ACTB*	qPCR-F	TTCTACAATGAGCTGCGTGTG
Human	*ACTB*	qPCR-R	GGGGTGTTGAAGGTCTCAAA
Human	*FZD7*	cloning-NotI-F	GCGGCCGCCACCATGCGAGACCCAGGTGCAG
Human	*FZD7*	cloning-AscI-R	GAGTGAGGCGCGCCTACCGCAGTCTCCCCCTTGC
Jellyfish	***EGFP***	cloning-AscI-F	TAGTATGGCGCGCCGGGTAGCAAGGGCGAGGAGC
Jellyfish	***EGFP***	cloning-BamHI-R	GAGGCAGGATCCTCACTTGTACAGCTCGTCCATGCCG

* also used for riboprobe cloning of *cachd1*

Table S6. Source of plasmids used as templates for *smo*- and *fzd-EGFP* flow cytometry, SPR and crystallography constructs.

Species	Gene	Construct ID	Source	Vector
Zebrafish	*fzd1*	IMAGE 9038402	Source Biosciences	pCR4-TOPO
Zebrafish	*fzd2*		Prof. Masa Tada (gift) *(80)*	
Zebrafish	*fzd3b*	IMAGE 7040422	Source Biosciences	pExpress-1
Zebrafish	*fzd4*	Synthesized clone ODa20912: XM_005173425	GenScript	pcDNA3.1+-DYK
Zebrafish	*fzd5*	IMAGE 9037464	Source Biosciences	pCR4-TOPO
Zebrafish	*fzd6*	IMAGE 6971142	Source Biosciences	pCMV-SPORT6.1
Zebrafish	*fzd7a*		Prof. Masa Tada (gift) *(81)*	
Zebrafish	*fzd7b*	IMAGE 5777452	Source Biosciences	pME18S-FL3
Zebrafish	*fzd8a*	IMAGE 7002555	Source Biosciences	pExpress-1
Zebrafish	*fzd8b*	IMAGE 6802128	Source Biosciences	pCMV-SPORT6.1
Zebrafish	*fzd9a*	Synthesized clone ODa11014: XM_003198686	GenScript	pcDNA3.1+-DYK
Zebrafish	*fzd9b*	IMAGE 9038534	Source Biosciences	pCR4-TOPO
Zebrafish	*fzd10*	IMAGE 7042011	Source Biosciences	pExpress-1
Zebrafish	*smo*		*(82)*	pCS2+
Mouse	$Cachd1_{ECD}$	IMAGE 6834428	Source Biosciences	pYX-Asc
Mouse	$Fzd5_{CRD}$	Synthesized clone	GenScript	pNeo_sec
Human	*FZD7*	IMAGE 4549389	Source Biosciences	pOTB7
Human	$FZD7_{CRD}$	Synthesized clone	GenScript	pNeo_sec
Human	$FZD8_{CRD}$	Synthesized clone	GenScript	pNeo_sec
Human	$LRP6_{P1E1P2E2}$	IMAGE 40125687	Source Biosciences	pHL_sec
Human	$LRP6_{P3E3P4E4}$	IMAGE 40125687	Source Biosciences	pHL_sec

Table S7. Riboprobe templates.

Gene	Vector	Resistance	Linearization	RNA Polymerase	Reference
aoc1	pCRII-TOPO	Amp, Kan	SpeI	T7	constructed
slc18a3b	pCRII-TOPO	Amp, Kan	XhoI	SP6	constructed
kiss1				T3	PCR-amplified
cachd1	pCRII-TOPO	Amp, Kan	SpeI	T7	constructed
zgc:101731	pCR-Blunt II-Topo	Kan, Zeocin	NotI	SP6	constructed
axin2	pSport 1	Amp	Asp718	SP6	*(83)*
selenop2	pBS KS+	Amp	SalI	T7	*(84)*
otx5	pBS	Amp	NotI	T7	*(8)*
kctd12.2	pBK-CMV	Kan	BamHI	T7	*(31)*
kctd8	pCRII-TOPO	Amp, Kan	XhoI	SP6	*(31)*
kctd12.1	pBK-CMV	Kan	EcoRI	T7	*(8)*
prss1	pCRII-TOPO	Amp, Kan	XhoI	SP6	*(85)*
spaw	pGEMT-EASY	Amp	SpeI	T7	*(86)*
lefty1	pBS SK+	Amp	NotI	T7	*(87)*
aldh1a3	pGEMT-EASY	Amp	SalI	T7	*(88)*
dbx1b	pCRII-TOPO	Amp, Kan	BamHI	T7	*(26)*
wnt3a	pBS	Amp	SmaI	T7	*(89)*
lef1	pCR-Blunt II-Topo	Kan, Zeocin	SacI	T7	*(90)*

Table S8. HCR probe sets for zebrafish *cachd1* and *lrp6*.

Gene	Amplifier	Name	Sequence
cachd1	B1	cachd1_B1_7	TTCTTGGATTGTTGGCGCAGGGTAA
cachd1	B1	cachd1_B1_8	AACTGCGGTAAACAGACCAGCATTA
cachd1	B1	cachd1_B1_9	GCGTCAAGGCATAGTTTTAGGCACT
cachd1	B1	cachd1_B1_10	TCCGGACTCCGGTAGGGTTACTAAG
cachd1	B1	cachd1_B1_14	CTGTCCGCGACCGACTCGCCATTGT
cachd1	B1	cachd1_B1_15	TCCACGCCGCGAAGGAGAATCGAGG
cachd1	B1	cachd1_B1_44	AGATTTTATCATGTTCGTCGATGGA
cachd1	B1	cachd1_B1_45	GAACAGTATCTGCTATCGTCAACAC
cachd1	B1	cachd1_B1_65	TGAAGGTGGCCACGTCGATCATTCG
cachd1	B1	cachd1_B1_66	CTCCCATCTGGTCCGCATAAGGCAA
cachd1	B1	cachd1_B1_82	CATAAACTATGCAGAGGATAAACGA
cachd1	B1	cachd1_B1_83	GCTGCTTCACCGGGATCTCTGGCTG
cachd1	B1	cachd1_B1_86	GAAGGCAGGAGCTGGGCTGCCCCAG
cachd1	B1	cachd1_B1_87	TCTCGACTGTAGCGAGCTGTTTAAA
cachd1	B1	cachd1_B1_88	TACCAGCGGACAACATCACCGTAGG
cachd1	B1	cachd1_B1_89	TCAGGTGCTCATAGGGAGAGGAGAA
cachd1	B1	cachd1_B1_91	TGTCGCTCAGGTAAGCAGTGTAGTG
cachd1	B1	cachd1_B1_92	GGCCGGGGTTGGCTATAAGTCGAGT
cachd1	B1	cachd1_B1_93	TCACCTCATTCCTCACAGAAGACTT
cachd1	B1	cachd1_B1_94	ATTCATCAGTCACGTGGCTGGTGGC
cachd1	B1	cachd1_B1_96	TGTAACGCCTCACAATGTAGCAGTT
cachd1	B1	cachd1_B1_97	TCCGCAGCACCCCATTGGGCGTTGC
cachd1	B1	cachd1_B1_98	CTTTGTCCATGAGTGAACCGGGGTA
cachd1	B1	cachd1_B1_99	ACCATTGCCTCCTGGTGGGATCGAA
cachd1	B1	cachd1_B1_103	TAGGGGCGTGGATGGTGTGGCTAAT
cachd1	B1	cachd1_B1_104	CTGTGTAACCAGAGGCCATTTGGGA
cachd1	B1	cachd1_B1_109	GGGCCACCAAATAGCCTCTGTCCTC

cachd1	B1	cachd1_B1_110	GACCCTTCGGATCAATCAGTGTCGG
cachd1	B1	cachd1_B1_120	AGAAGGCCAGCGCATCACACGTCTC
cachd1	B1	cachd1_B1_121	AGAGACGGTCCACAGTACTGCAAGC
cachd1	B1	cachd1_B1_126	AAGGCTCCTGGTGCACGTCACAGCT
cachd1	B1	cachd1_B1_127	GACTGGGCTCAATTACAGTCAAAGA
cachd1	B1	cachd1_B1_134	CATAAGGACTCTTGGCGCCCACTAT
cachd1	B1	cachd1_B1_135	CCTCATCTAAAATGCCCATTCCATC
cachd1	B1	cachd1_B1_139	GGTGCCTATAGGCATAAACTGCCAA
cachd1	B1	cachd1_B1_140	TGTGCTGATGACTGCGACGGTGGAT
cachd1	B1	cachd1_B1_150	CCGCTGAGAGAGGATCGTTATTGCA
cachd1	B1	cachd1_B1_151	CCTCGTCGTGATTGCCCACATCAAC
cachd1	B1	cachd1_B1_168	ACCTTTACGGGCCTGAGAAAAGCTG
cachd1	B1	cachd1_B1_169	ACAAAACCAGGGCTGGGTACTAAAA
lrp6	B5	lrp6_B5_9	TAAACAGCGTCCGTTTAATAGACTC
lrp6	B5	lrp6_B5_10	TCTGAACGCCGCTGGGCGCCGAGCC
lrp6	B5	lrp6_B5_20	CCACGATGACAGAGCGCAGCGACCC
lrp6	B5	lrp6_B5_21	GGCCGTTGGGCCAGTAGATCTCCGT
lrp6	B5	lrp6_B5_31	GCTGGCTGTAGACGTGGATGTCCAT
lrp6	B5	lrp6_B5_32	GGCTCGCCACGTCCATGGGCTGGCG
lrp6	B5	lrp6_B5_35	TTGGACAGGCGCACTGATAGTAGGG
lrp6	B5	lrp6_B5_36	TGTGGTCCTCCAGCAGCTGTACGCC
lrp6	B5	lrp6_B5_38	CTGTGCGGCGCGCTAGCAGGAGGAG
lrp6	B5	lrp6_B5_39	GCGTGTCCAGAGAGATCCGGCGCAG
lrp6	B5	lrp6_B5_45	GCGAGGTCACCACCAGCTGAGCGTC
lrp6	B5	lrp6_B5_46	CGGCGATGCCGTCCGGGTGGTTCAC
lrp6	B5	lrp6_B5_66	TCACCCCGAAGGTCTGGTGGACGAA
lrp6	B5	lrp6_B5_67	AGCCGCCATTAGCCCACGCACACGG
lrp6	B5	lrp6_B5_87	CCATCGCTGCACGGTCTATCTTGGG
lrp6	B5	lrp6_B5_88	GCACCAGAGTGATGCGGCCCGACCC

lrp6	B5	lrp6_B5_113	CGAGGTTTGAGCCGCCAACAGCGCC
lrp6	B5	lrp6_B5_114	CGATGCTCAGGTCGTACGGCTGCAG
lrp6	B5	lrp6_B5_126	CGCTGCTCTCGATGCGCCGCAGGTC
lrp6	B5	lrp6_B5_127	TCACAATCCGATTGGCTCCGGACAG
lrp6	B5	lrp6_B5_132	GCGCCTGTATTTTGGTTCGTCCCTC
lrp6	B5	lrp6_B5_133	CGTGGATGTCGCTCAGTGAGGCGAT
lrp6	B5	lrp6_B5_141	GGATACAGTCCACCTCACCCGACAC
lrp6	B5	lrp6_B5_142	CAAACCCGTCACAGCGCCACGCCTG
lrp6	B5	lrp6_B5_147	CGTCGGAGCGGTCCTGGCAGTTGAT
lrp6	B5	lrp6_B5_148	CAGGGCACAGAACTTCACACTTGTT
lrp6	B5	lrp6_B5_152	CTGTCGCATAGCAGCCGATCTCGTC
lrp6	B5	lrp6_B5_153	TGTTAGTGGGAGCAAACGACGGCTC
lrp6	B5	lrp6_B5_155	ACACCGCGCCGACCACGAACAGCAC
lrp6	B5	lrp6_B5_156	GGCAGAGCACGCGCTGGCACACGAA
lrp6	B5	lrp6_B5_158	GTCCGTGAACCACGAAGTCATTGGT
lrp6	B5	lrp6_B5_159	GGACGTATCCCAGCGGCACCGGCGG
lrp6	B5	lrp6_B5_162	CTCCCATGATGCTCAGCGAGCCCAT
lrp6	B5	lrp6_B5_163	CGCGGTCGTACGGTGGTCCACTGCT
lrp6	B5	lrp6_B5_170	CGAAGTGGCGGTAACTGTACGGCCG
lrp6	B5	lrp6_B5_171	CCGTGCTGCACGGCGTCGTCGGAGG
lrp6	B5	lrp6_B5_175	GCAGCGGCTCCGAGTCGTAGTTCAG
lrp6	B5	lrp6_B5_176	ACTGGCTGCGCGGCGTGGGCGGCGG
lrp6	B5	lrp6_B5_178	GCTCGGTGTACGGTGACGGCGGGCA
lrp6	B5	lrp6_B5_179	GCGGGTACAGCTGGTGCGAGTAGCT